The Thesis Committee for Ann Caroline Bovay
Certifies that this is the approved version of the following thesis:

New Models of Early Cretaceous Source-to-Sink Pathways in the Eastern Gulf of Mexico

APPROVED BY
SUPERVISING COMMITTEE:

Supervisor: _____
Ronald J. Steel

Co-Supervisor: _____
John W. Snedden

_____
David Mohrig

New Models of Early Cretaceous Source-to-Sink Pathways in the Eastern Gulf of Mexico

by

Ann Caroline Bovay, B.S.

Thesis

Presented to the Faculty of the Graduate School of

The University of Texas at Austin

in Partial Fulfillment

of the Requirements

for the Degree of

Master of Science in Geological Sciences

The University of Texas at Austin

May 2015

Dedication

I dedicate this thesis to my mother, who always loves me, and provided many study breaks to talk about wedding planning throughout the last eighteen months.

Acknowledgements

I would like to acknowledge my research supervisor, Dr. John Snedden, for your patient teaching and sharing so many insights from your entire career with me. John pushed me to think beyond the workstation and taught me how to really think on a regional scale. Thank you for supporting my desire to add the detrital zircon analysis to this study. I am so appreciative of the opportunity to learn this methodology and feel that the experience epitomizes what graduate studies should be. Thanks to Ron Steel for asking me the right questions to further my research and keeping me on track. The field trip in your Clastic Depositional Systems class was one that really make things click for me and I am so grateful to have been able to participate. Thank you to David Mohrig for your encouragement throughout 3D Stratigraphy and the Field Stratigraphy of Southwest Oregon, which were my favorite classes in the Jackson School. The lessons learned in both courses have proven to be influential already.

I appreciate the help of Patty Ganey-Curry, the project manager of the Gulf Basin Depositional Systems project, for organizing our sponsor meetings which gave me such practical experience as making technical presentations in front of hundreds of scientists. Thank you for the everyday support, banter, walk breaks, and fun.

Thank you to the graduate and undergraduate students and staff of GBDS for your support and laughter, especially Jie Xu, who spent countless selfless hours guiding me through the U-Pb detrital zircon analysis process, from sampling in Tallahassee to the final data processing. Thank you to Danny Stockli for allowing me to use your lab to accomplish the U-Pb dating with open arms.

Thank you to the geoscience team of TGS for taking me under your wing and not only providing me with an excellent data set, but providing support along the way, including reviewing my interpretation. Thank you Brad Torry, Jason Kegel, and Melanie Blind especially.

I would acknowledge the generous staff at the Florida Geological Survey in Tallahassee for allowing me to visit your facilities twice and collect samples. It was a wonderful journey for me to return home to Florida for geological research. Thank you to Jesse Hurd and David Paul for your gracious assistance leading up to and during my two visits.

I appreciate the numerous sponsors of the GBDS project. Your support has greatly influenced my graduate studies, from a day-to-day experience, to extremely helpful insights at our meetings, and I look forward to interacting with you throughout the rest of my career.

Thank you to my friends here at the Jackson School. I have enjoyed learning from you and with you. Thank you for the fun we have had here in Austin!

To my parents, thank you for your constant encouragement and support. Thank you for adapting to short phone calls on the way to work and class. Thank you for pushing me to the end. Thank you for giving me more hours to work by taking care of our sweet beagle, Derby, in my final semester.

Lastly, thank you to my amazing fiancé, Thomas, for supporting me each day, no matter how crazy I am from looking at seismic for hours on end. You uplift me and balance me.

Abstract

New Models of Early Cretaceous Source-to-Sink Pathways in the Eastern Gulf of Mexico

Ann Caroline Bovay, M. S. Geo Sci

The University of Texas at Austin, 2015

Supervisors: Ronald J. Steel and John W. Snedden

During the early Cretaceous (Valanginian-Hauterivian stages), there were significant basin- to regional scale changes in the Gulf of Mexico affecting marine tectonics, terrestrial erosion, and sedimentation on the Florida shelf and in the eastern Gulf of Mexico deep-water areas. Termination of Gulf of Mexico (GOM) sea-floor spreading left its tectonic mark at the beginning of the Valanginian stage. Subsequent uplift of the Florida Ocala Arch caused a source terrane to perch above the landscape, leading to erosion and transport of siliciclastics across the shelf and into the GOM deep-water as a sandy progradational delta-fed slope apron. Contemporaneous supply from an Appalachian source terrane brought additional siliciclastic material into the GOM DeSoto Canyon-Mississippi Canyon deep-water off the Florida coast.

To augment the results of seismic mapping of 2D and 3D narrow azimuth (NAZ) seismic reflection surveys, the Hosston interval of the onshore Florida Stanolind Sun Perpetual Forest #1 well was sampled and U-Pb detrital zircon analysis performed at Dr. Danny Stockli's geochronology lab at The University of Texas at Austin. Results indicate

Hosston siliciclastics were derived from the Suwannee Terrane and the Trans-Amazonian/Eburnean craton, rather than the Grenville Province of the Appalachian Mountains. For this Valanginian-Hauterivian-age Hosston sand grains to reach the deep-water and deposit a progradational sandy delta-fed apron of 200 km in length, we interpret submarine canyons incised the shelf edge, bringing both the carbonate reef rim material and siliciclastic material from where open shelf passages exist, down to the deep-water through turbidity flow processes.

The Mississippi Canyon protraction block asymmetric expulsion rollovers, salt tectonic features which preserve direction of large-scale sedimentary progradation and basin filling, indicate the Hosston material was deposited in an ENE-WSW direction, or derived from an Appalachian source terrane. Scaling relationships between river channel length and fan length help constrain the possible extent of the Appalachian-sourced fan, resulting in the most likely fan runout length of approximately 70 km.

Seismic observations, new interpretations of onshore and offshore Gulf Basin Depositional Synthesis project-digitized wells, and results of U-Pb detrital zircon dating support construction of an updated Hosston paleogeographic map, focusing on the eastern Gulf of Mexico where both economic and scientific interests coincide.

Table of Contents

List of Tables

List of Figures

Chapter 1: Introduction and Geologic Background

INTRODUCTION

The goal of this study is to characterize Early Cretaceous (Valanginian-Hauterivian)-aged sandy deposits in the eastern Gulf of Mexico (GOM). Depth-imaged 2D and 3D seismic data, well log correlation, sand grain size measured from Valanginian-Hauterivian intervals of the cores of a key well, and detrital zircon U-Pb dating of aforementioned grains allow for characterization and source-to-sink analysis of Early Cretaceous deep-water deposits, as well as a new depositional model of Valanginian-Hauterivian siliciclastics previously investigated only in the western GOM onshore areas.

The Valanginian-Hauterivian age deposit named the Hosston Formation (coeval to the Travis Peak Formation in Texas) lies conformably atop the Berriasian age Cotton Valley Knowles Formation and below the Barremian-Aptian age Sligo Formation (coeval to Pettet Formation in Louisiana). The Travis Peak Formation in onshore areas is interpreted as a delta-fringe, fluvial, flood-plain, and coastal-plain succession (Figure 1; Dyman and Condon 2006). The Sligo Formation is a carbonate platform reef that rimmed the entire northern half of the GOM. Previous studies define the Sligo-Hosston contact as gradational and do not identify a seismically-resolved reflection boundary. Ewing (2010) separated the Travis Peak of south Texas interval into a basal lowstand wedge and a main transgressive systems tract model, an idea which is tested for the eastern Hosston in this study.

To date, Valanginian-Hauterivian age hydrocarbon reservoirs are produced only in the western GOM onshore setting, and research has been focused there. The eastern deep-water Gulf of Mexico exploration focus on the Jurassic Norphlet, Smackover, Haynesville, and Cotton Valley formations. Provenance studies in the eastern Gulf have emphasized the Jurassic reservoirs as well. Consequently, we have much to learn about the Valanginian-

Hauterivian age in the eastern Gulf of Mexico. We believe the Valanginian-Hauterivian is an important time interval to investigate for future hydrocarbon exploration and to place in the context of the evolution of the Gulf of Mexico basin as a whole.

This study is the first, to our knowledge, to demarcate a seismic boundary between the siliciclastic Hosston and overlying carbonate Sligo Formations and to incorporate detrital zircon provenance analysis in the eastern Gulf for this interval. Not only does this study offer a seismic interpretation of the Valanginian-Hauterivian age deposits but provides insight into a previously overlooked Florida Peninsula source terrane.

The Mississippi Canyon OCS protraction block is known to contain asymmetric expulsion rollover salt features. We aim to determine the relative age of the deposits and how their formation relates to the evolution of the eastern Gulf of Mexico.

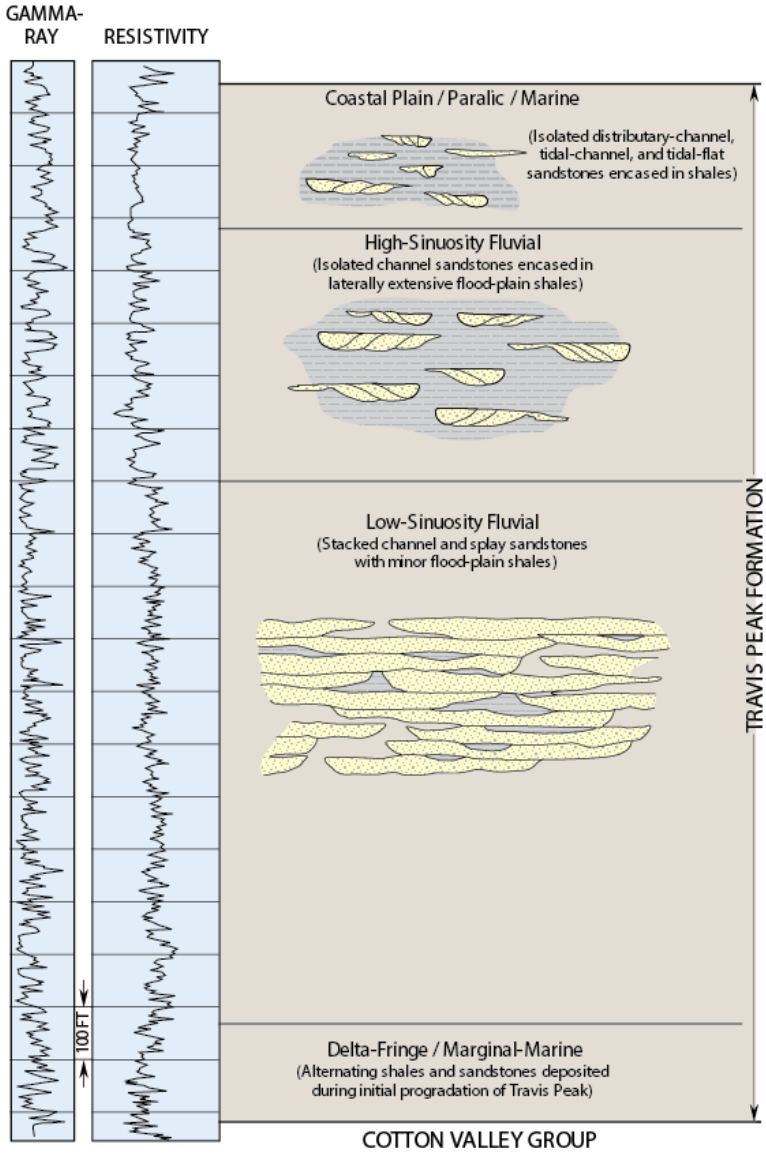

Figure 1: Type log of the Travis Peak Formation of east Texas shown with interpreted depositional environments of the four main sequences. 100 ft depth increments on log. (From Dyman and Condon, 2006).

REGIONAL BACKGROUND OF THE EARLY CRETACEOUS GULF OF MEXICO BASIN

The early Cretaceous eastern offshore GOM is defined as the shelf and deep-water from Florida to the eastern part of Louisiana. This study focuses on the deposits found from Tortugas Valley to Mississippi Canyon OCS blocks. Known sediment source terranes of

the early Cretaceous deposits Gulf-wide are the Appalachian Mountains to the east and the Rocky Mountains to the west (Dyman and Condon 2006). Major known sediment transport systems of the early Cretaceous include the ancestral Mississippi and Red Rivers.

Seismic refraction data collected by the 2010 Gulf of Mexico Basin Opening (GUMBO) Program (Christeson et al, 2013; Eddy et al., 2013; van Avendonk et al., 2013), when paired with seismic reflection data over the same profiles, sheds light on the temporal evolution of the eastern GOM (Snedden et al., 2013). This data suggests the GOM basin opens in the Middle Jurassic, with the Smackover-Norphlet supersequence as the last pre-spreading deposits (Snedden et al., 2013). Snedden et al. (2013) have interpreted the termination of sea-floor spreading in the eastern GOM to be coeval with the initiation of Valanginian-Hauterivian Hosston deposition 133-138 Ma. (Figure 2).

The early Cretaceous deposits were preceded by important formations which influenced the early Cretaceous paleotopography and bathymetry. The Louann salt, deposited in the Middle Jurassic (Callovian stage), creates many challenges with understanding the geology of the GOM as well as many opportunities for trapping hydrocarbons. The autochthonous, parautochthonous, and allocthonous salt, as well as its evacuation features, affects seismic interpretation of the Valanginian-Hauterivian Hosston in the western part of this study in Mississippi Canyon (Herron, 2014).

In areas where the Louann salt was present, the Jurassic (Oxfordian) Norphlet Formation was deposited conformably on top of the Louann salt (Mancini et al., 1985). Where the Louann salt was not deposited, the Norphlet Formation was deposited unconformably on the older Eagle Mills formation, Werner formation, Mesozoic volcanics, or Paleozoic rocks (Mancini et al., 1985). The Norphlet Formation is best known for its eolian desert plain sandstone deposits that thicken from onshore Alabama to Mobile Bay (Marzano et al., 1988).

After deposition of the Norphlet, Late Oxfordian-age Smackover carbonates formed in a marine transgression (Mancini et al., 1990). The Kimmeridgian brought about hypersaline sabkha and lagoon environments (Buckner Anhydrite) behind a shelf margin reef (Gilmer Limestone) of the Haynesville Formation (Moore, 1984; Salvador, 1987; Mancini et al., 1990).

The Cotton Valley-Bossier supersequence was deposited in the Tithonian-Berriasian (late Jurassic-early Cretaceous) and the Cotton Valley-Knowles supersequence was deposited in the Berriasian age. The Bossier shale underlies the Cotton Valley Terryville massive sandstone complex of onshore Texas and Louisiana, containing the Schuler Formation and the Hico shale (Coleman, Jr. and Coleman, 1981). The Cotton Valley Knowles limestone was then deposited conformably atop the Terryville complex (Coleman, Jr. and Coleman, 1981). The Cotton Valley Knowles reef system extended along part of the northern GOM, including DeSoto Canyon.

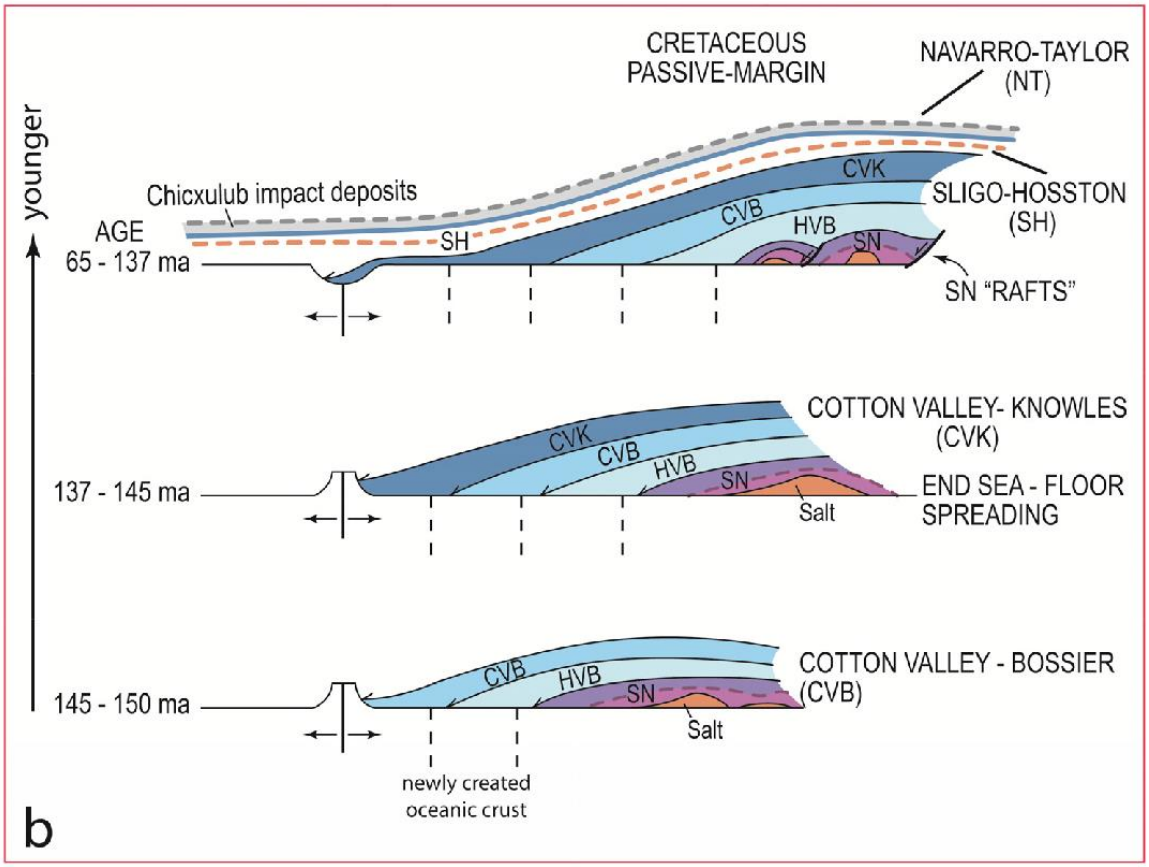

Figure 2: Schematic temporal evolution of the eastern Gulf of Mexico with respect to the Gulf of Mexico spreading center: Cotton Valley-Bossier to Navarro-Taylor deposition. (Modified from Snedden et al., 2013).

TRAVIS PEAK FORMATION: VALANGINIAN-HAUTERIVIAN EQUIVALENT IN THE WESTERN GULF OF MEXICO

The Valanginian-Hauterivian Travis Peak/Hosston formation of onshore Texas, southern Arkansas, Louisiana, and Mississippi is a basinward-thickening wedge of clastic material derived from fluvial-deltaic depocenters in east Texas and western Mississippi, sourced by the ancestral Red River and ancestral Mississippi River (Figure 3). Dyman and Condon (2006) report three stratigraphic intervals in the Travis Peak, based on the findings of Saucier (1985) and Saucier et al. (1985): (1) basal interval of mixed sandstone and shale, representing delta-fringe deposits; (2) thick middle section of stacked, aggradational

braided stream sandstones, representing high-sinuosity fluvial and flood-plain deposits; (3) upper interval of sandstones and mudstones, representing coastal plain/paralic/marine deposits (Figure 1).

The basal interval of the Travis Peak has high mudstone content and isolated sandstone packages, interpreted to represent delta-fringe deposits (Dyman and Condon, 2006). The basal section grades into the main, thick interval of the Travis Peak (Dyman and Condon, 2006). The braided sandstones of the middle section are characterized by blocky spontaneous potential (SP) log curve response and on the basis of sandstone body geometries and bedforms observed in core (Dyman and Condon, 2006). The amalgamated braided stream sandstones, lacking shales, can occur as massive sandstone units up to 250 feet thick (Dyman and Condon, 2006; Saucier, 1985). The middle interval has a gradational contact with the overlying upper unit in which thick mudstones separate individual sandstones (Dyman and Condon, 2006). The coastal-plain deposits, interpreted from thin, serrated, coarsening-upward or thinning-upward SP log responses, interfinger with and are overlain by the Sligo (Pettet) carbonate formation (Dyman and Condon, 2006).

The Travis Peak and Hosston reservoirs of Texas, Arkansas, Louisiana, and Mississippi are believed to be sourced by the late Jurassic Bossier Shale and the late Jurassic Smackover carbonate mudstones (Figure 4; Dutton, 1987). The thick mudstones of the upper Travis Peak interval serve as adequate hydrocarbon seals for the primary high-sinuosity, fluvial-channel sandstone and the tidal-channel and tidal-flat sandstone reservoirs from the coastal plain (Dyman and Condon, 2006; Tye, 1989; Dutton, Laubach, and Tye, 1991).

Travis Peak porosity and permeability are greatly influenced by diagenesis, including: (1) mechanical compaction; (2) precipitation of quartz, dolomite, chlorite, illite, and ankerite; (3) dissolution of feldspar leading to secondary porosity; (4) reservoir

bitumen formation (Dyman and Condon, 2006; Dutton and Diggs, 1992). Mechanical compaction decreased porosity in the Travis Peak until a burial depth of 3000 feet when widespread quartz cementation became the dominant process for the next 2000 feet of burial (Dyman and Condon, 2006). Secondary porosity was generated by the dissolution of feldspar, but porosity was reduced by precipitation of authigenic chlorite, ankerite, and illite until a burial depth of 7500 feet (Dyman and Condon, 2006). Reservoir bitumen lined and filled primary and secondary pores in the Travis Peak sandstones, further reducing porosity and permeability (Dyman and Condon, 2006; Dutton et al., 1991; Lomando, 1992).

Ewing (2010) identifies an atypically sandstone-rich basal Hosston in south Texas including a prograding base, aggrading alluvial plain, and a transgressive sandstone top, conformably overlain by a thick, continuous shale. Ewing (2010) argues the basal Hosston is a lowstand systems tract deposit overlying a major sequence boundary (at the Cotton Valley contact; Figure 5). With the deltaic and shoreline systems lowstand deposits identified, Ewing (2010) suggests the potential for a lowstand fan to exist as a downdip exploration target. Interpretation of well logs and seismic data at Valanginian-Hauterivian-Hosston time in the eastern Gulf of Mexico in this study is guided by this notion of a main, upper Hosston and a secondary, basal Hosston of high sandstone content. The related question of whether or not the basal Hosston is present in the eastern Gulf deep-water will be addressed in the Chapter 4: Discussion.

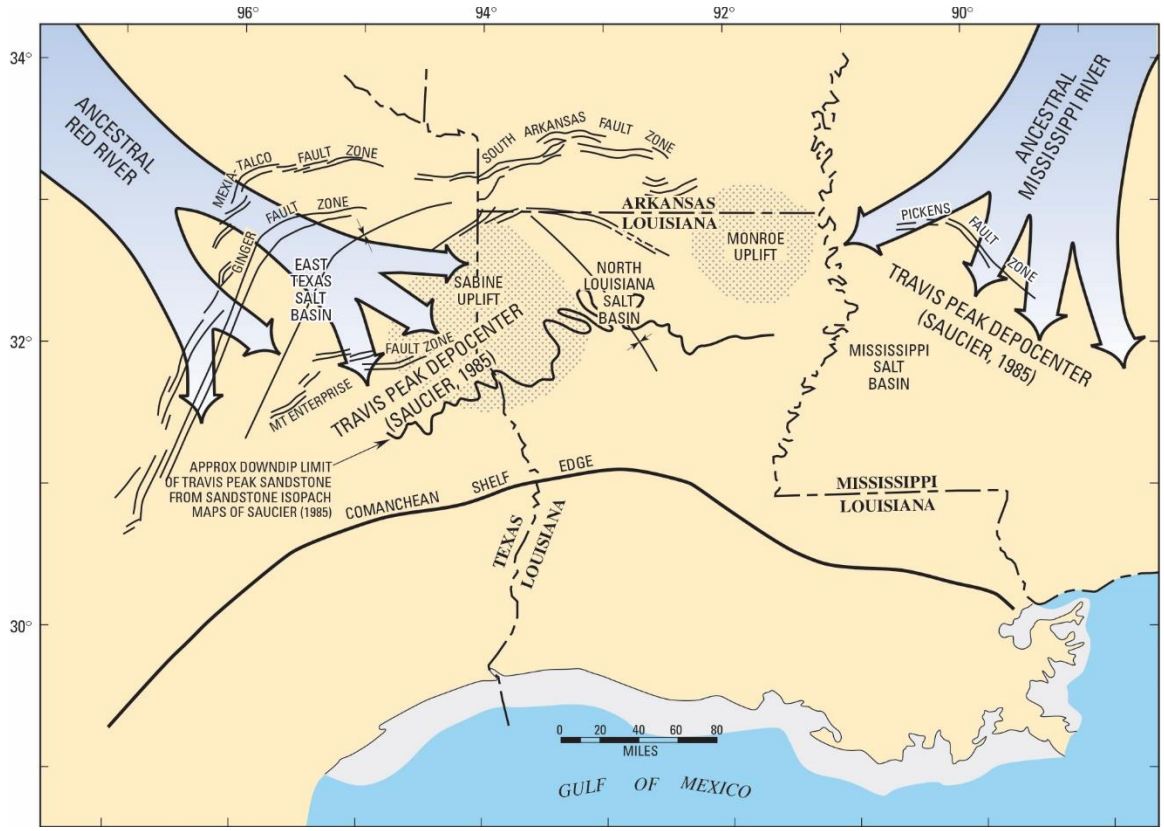

Figure 3: Map of Early Cretaceous Travis Peak formation depocenters of the northern Gulf of Mexico. The Travis Peak formation is the Valanginian-Hauterivian equivalent of the Hosston formation of the eastern Gulf of Mexico. (From Dyman and Condon, 2006).

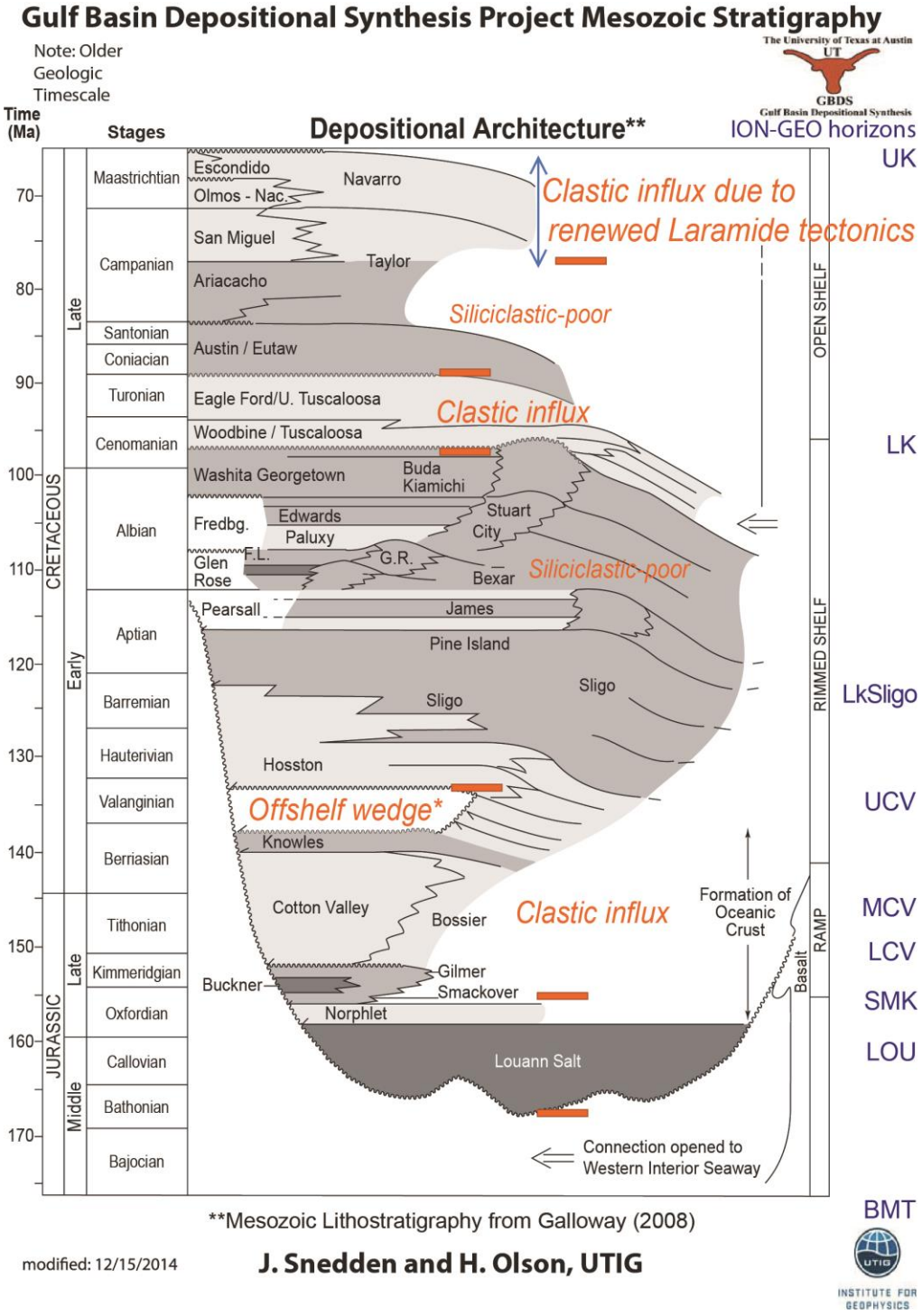

Figure 4: Mesozoic Stratigraphy of Gulf of Mexico, modified from Snedden and Olson (pers. comm.). Orange bars indicate boundary between siliciclastic influx and siliciclastic-poor intervals.

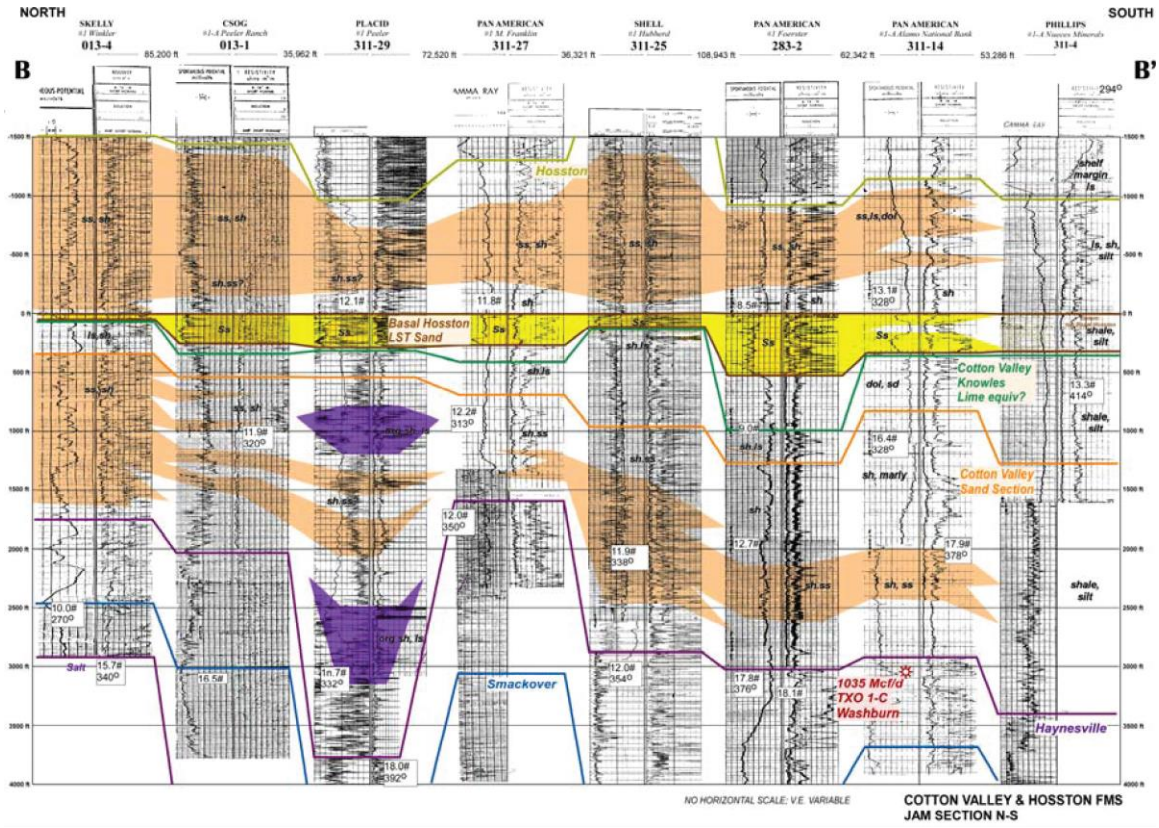

Figure 5: North-south dip stratigraphic cross section from south Texas of the Hosston and Cotton Valley formations, hung on the top of the basal Hosston. (From Ewing, 2010).

HOSSTON IN MEXICO

Mexico offers outcrops of the Texas subsurface and a wealth of information on deposition from the upper Triassic to the lower Cretaceous (Wilson et al., 1981). The Valanginian-Hauterivian deposition in Mexico ranges from limestone, to limestone and shale, to sandstone and shale in three different formations, called the lower Tamaulipas, Taraises, and La Casita (Wilson et al., 1981). The La Casita sandstone and shale formation is well studied in the Sierra Madres south of Saltillo. Wilson et al. (1981) divide La Casita into three units: (1) the mudstone and siltstone unit representing prodelta deposits; (2) the

fining upward and coarsening upward unit representing lower-fan to shallow marine deposits; (3) the fine sand unit representing waning coarse sediment input.

The lowest unit, representing the prodelta deposits, is interpreted to have collected on the shelf before the input of coarser sediment (Wilson et al., 1981). They believe the lower-fan to shallow marine deposits were deposited at the fan-delta's most basinward position in both streams distal to the alluvial fan (fining-upward) and coastal and shelf environments (Wilson et al., 1981). The unit contains multiple coarsening-up sequences, indicating frequent delta lobe shifting and progradation (Wilson et al., 1981). Rapid deposition is interpreted based on the mineralogical and textural immaturity of the unit (Wilson et al., 1981). The upper, waning coarse sediment input unit represents deposition in which only fine sediment was transported to the shelf (Wilson et al., 1981).

BIOSTRATIGRAPHY

The Gulf Basin Depositional Synthesis Project (GBDS) at The University of Texas at Austin Institute for Geophysics considers biostratigraphy to be part of the trinity of regional interpretation and synthesis of the Gulf of Mexico, in addition to well logs and seismic reflection data. Our research group has identified an extensive collection of benthic foraminifera, planktonic foraminifera, ostracods, dinoflagellates, and calcareous nannofossils associated with Mesozoic stratigraphy (Olson et al., in press). The type biostratigraphic section for the Hosston formation in this study includes biostratigraphy tops from multiple wells in the Destin Dome and DeSoto Canyon offshore protraction blocks (Figure 6). The United States Department of the Interior Bureau of Ocean Energy Management (BOEM) Paleo for Public Release Report for the Chevron Destin Dome 422 #1 well (API 0608224002000) contains a definite within Barremian call with the identification of *Clavihedbergella eocretacea* planktonic foraminifera, identified by Olson

et al. (pers. comm.) to be within the third GOM-local Barremian chronostratigraphic surface (Figure 7). The BOEM Paleo for Public Release Report for the Shell DeSoto Canyon 269 well (API 0608234000600) contains a definite top Barremian call with the identification of *Calcicalathina oblongata* nannofossil as well as a definite top Hauterivian call with the identification of *Cruciellipsis cuvillieri* nannofossil, identified by Olson et al. (in press) to be within the first GOM-local Barremian chronostratigraphic surface and fourth GOM-local Hauterivian chronostratigraphic surface, respectively (Figure 7). The BOEM Paleo for Public Release Report for the Chevron Destin Dome 422 #1 well (API 0608224002000) contains a definite top Berriasian call with the identification of *Schuleridea acuminata* ostracod as well as a definite top Berriasian call with the identification of *Hutsonia vulgaris* ostracod, identified by Olson et al. (in press) to be within the eighth GOM-local chronostratigraphic surface (Figure 7). The BOEM Paleo for Public Release Report for the Shell DeSoto Canyon 269 well (API 0608234000600) contains a definite within Berriasian call with the identification of *Polycostella beckmannii* nannofossil, identified by Olson et al. (pers. comm.) to be within the first GOM-local Berriasian chronostratigraphic surface (Figure 7). The Shell DeSoto Canyon 268 #1 ST00BP02 well (API 0608234001702) contains the same BOEM biostratigraphy calls as the Shell DeSoto Canyon 269 well. With high confidence, we can constrain the Hosston formation to the top of the Hauterivian and stratigraphically above the Cotton Valley Knowles supersequence, which terminates with the second GOM-local Valanginian sequence boundary. Many of the BOEM Paleo for Public Release Reports contain Hauterivian and Valanginian calls that are not included in the GBDS Mesozoic Biostratigraphy Chart, but are used in coordination with well log and seismic reflection data as interpretation allows.

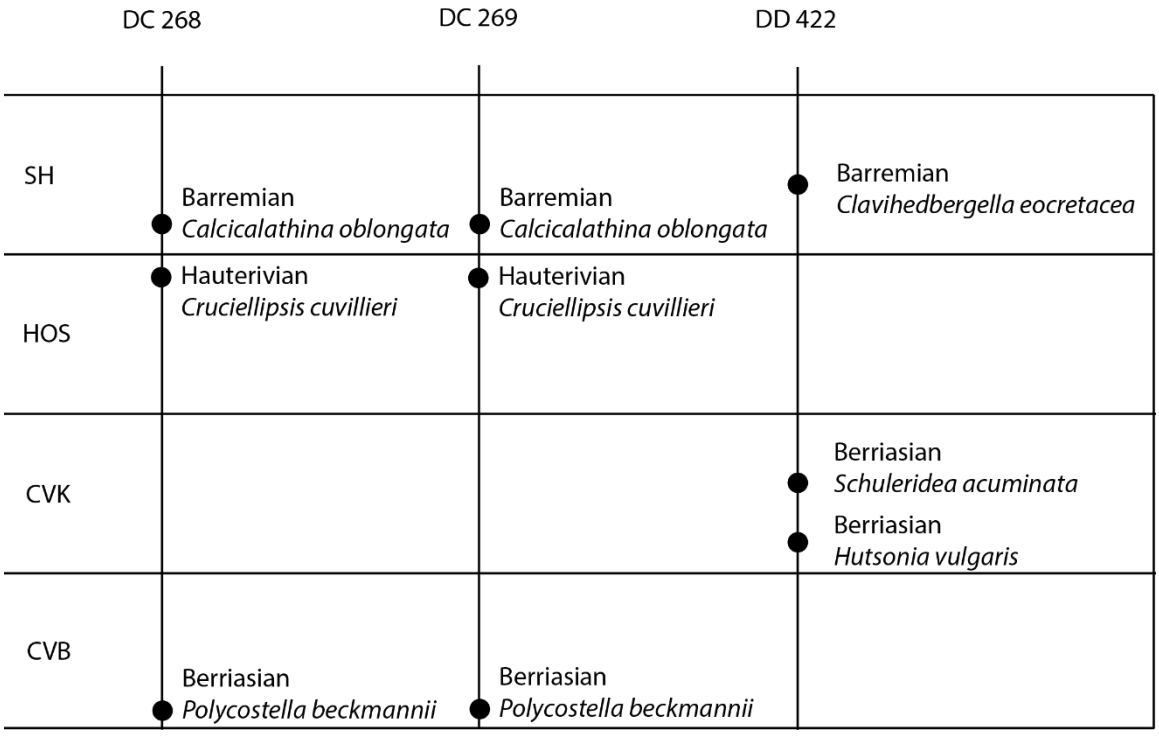

Figure 6: Type biostratigraphy of Hosston formation used throughout study, after biomarkers identified in BOEM Paleo for Public Release Reports were matched to the GBDS Mesozoic Biostratigraphy Chart and Olson et al., in press.

Gulf of Mexico Mesozoic Biostratigraphy Table

Figure 7.

Figure 7: Gulf Basin Depositional Synthesis Project Mesozoic Biostratigraphy of Sligo-Hosston supersequence. BOEM biostratigraphy calls are compared against the GBDS Mesozoic Biostratigraphy Chart, and then against well logs and seismic reflection data by GBDS researchers. The Hosston formation is considered in this study to extend from the Valanginian age to the Hauterivian age. (Modified from Olson et al., in press).

SOURCE-TO-SINK SYSTEMS OF THE EARLY CRETACEOUS EASTERN GULF OF MEXICO

Somme et al. (2009) define the source-to-sink system as all elements within an "erosional-depositional system" that are a factor in sediment erosion, transport, and deposition, from the catchment headwaters to the deep-water basin floor fan. Genetically related segments comprise the system so that erosional or depositional change to one component of the system is reflected by adaptation by one or more adjacent segments (Figure 8; Somme et al., 2009; Moore, 1969). The source-to-sink system encompasses both sedimentological – in sediment storage, buffering, and transfer – and morphological – in segment gradient, length, and area – components of an erosional-depositional system (Somme et al., 2009). Somme et al. (2009) build upon the important work of numerous predecessors on individual segments of the source-to-sink system (the catchment, shelf, slope, and basin floor) to compose a global database of large-scale relationships within and between source-to-sink systems as a whole, and has been used by other authors since (Blum and Pecha, 2014).

It is accepted that in general, a large catchment area generates higher sediment yield than a small catchment area, and Somme et al. (2009) explore similar relationships within many segments of the source-to-sink system based on their global database. Somme et al. (2009) compare river channel length and fan length, finding a strong relationship between these two segments of the source-to-sink system, especially in small tectonically active systems (Figure 9). Another relationship derived from Somme et al.'s (2009) work is that of catchment area and basin floor fan area: in small systems, the catchment segment is twice as long as the basin floor segment; in medium and large systems, whether passive, active, or mixed, the catchment segment is three or four times as long as the basin floor segment (Figure 10). These scaling relationships defined by Somme et al. (2009) are used in this study to establish a framework for two source-to-sink systems of the early

Cretaceous of the eastern Gulf of Mexico in order to characterize the potential for basin floor fan and sandy apron sinks.

The eastern Gulf of Mexico paleoslope and deep-water is considered a sink for siliciclastic deposits which originated in the Appalachian Mountains. Previous publications suggest that the Florida Peninsula itself was a paleotopographic high, which leads us to consider it as a source terrane for the Valanginian-Hauterivian siliciclastics in addition to the Appalachians (Winston 1976; Scott 1988). Sea-floor spreading in the eastern GOM led to the uplift of the northern Florida Peninsula where the Suwannee Basin once existed. This Ocala Arch would have been primed for erosion at the termination of sea-floor spreading at the Valanginian age. This study investigates the Ocala Arch as a previously overlooked proximal source terrane for siliciclastic deposits in the eastern GOM, challenging the notion that the Appalachians serve as the source terrane for early Cretaceous siliciclastic deposits in the eastern GOM.

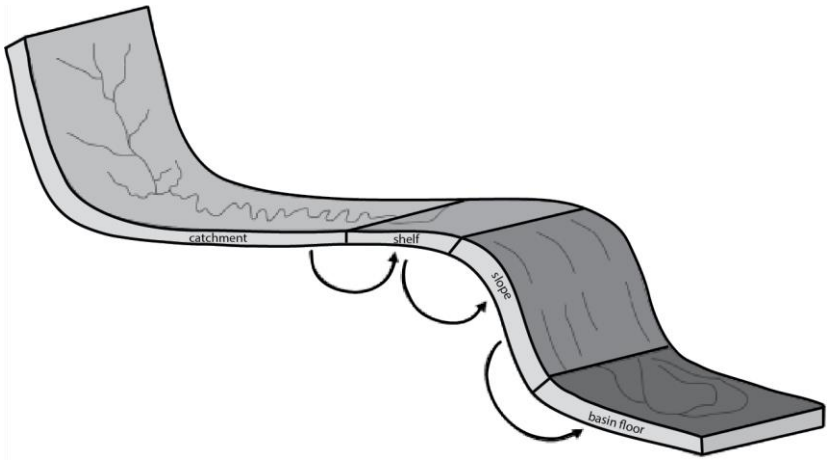

Figure 8: The four genetically-related components of the source-to-sink system: catchment, shelf, slope, and basin floor. (From Somme et al., 2009).

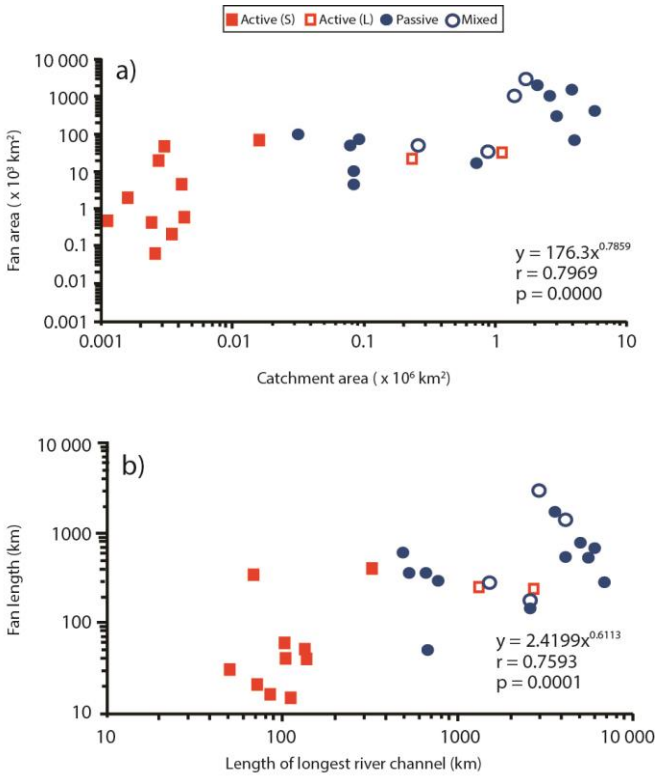

Figure 9: Scaling relationships found between morphological components of the segments of the source-to-sink system, according to type of continental margin at the location of each system: tectonically active (S=small, L=large), passive, and mixed. a) Catchment area vs. Fan area b) Length of longest river channel vs. Fan length. (Modified from Somme et al., 2009).

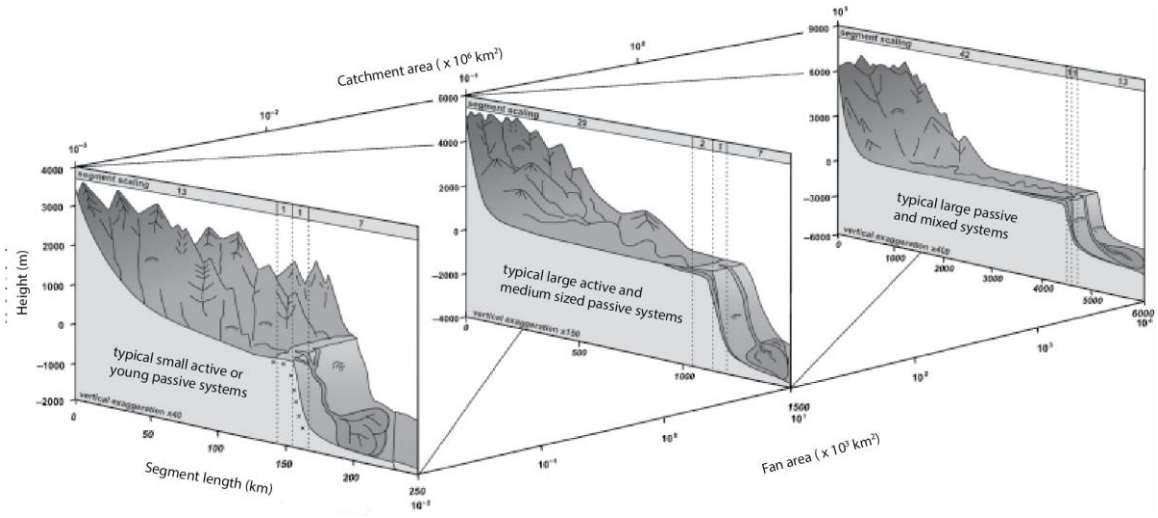

Figure 10: Depiction of scaling relationships between the basin floor, shelf, and catchment segments of the source-to-sink system and the slope length. A key general relationship: as shelf, slope, and basin floor become larger, so does the catchment. (From Somme et al., 2009).

ASYMMETRIC EXPULSION ROLLOVERS

An asymmetric expulsion rollover is a salt tectonic feature that preserves the sediment progradation direction despite alteration caused by the salt tectonics (Ge et al., 1997). Assuming salt is deposited in a nearly flat layer (for example, the Callovian-aged Louann salt in the Gulf of Mexico), a subsequent horizontal deposit of sediment is laid conformably on top of the salt (such as the Cotton Valley Bossier Supersequence). As sediment continues to be deposited, and sourced from a particular location and direction, weight of the sediment causes differential loading, and the underlying salt begins to move, generally in the direction of progradation, forming a mound or dome-shaped salt feature. Sediment onlaps onto the structure until eventually the prograding sediment is deposited over top of the salt dome. When the salt evacuates, or is expelled, to form an overlying salt canopy, for instance, the sediment structure collapses and forms rollovers resulting in what looks like downlapping stratal terminations. As opposed to a turtle structure, in which the

salt evacuation feature creates symmetric rollover-type structures, only the landward side of an asymmetric expulsion rollover originally onlapping onto the salt structure creates the rollover structure, thus termed asymmetric (Ge et al. 1997; Hudec, pers. comm.; Figure 11). Information on the timing and orientation of asymmetric expulsion rollovers in Mississippi Canyon help constrain the Valanginian-Hauterivian paleogeography of the eastern Gulf of Mexico in this study.

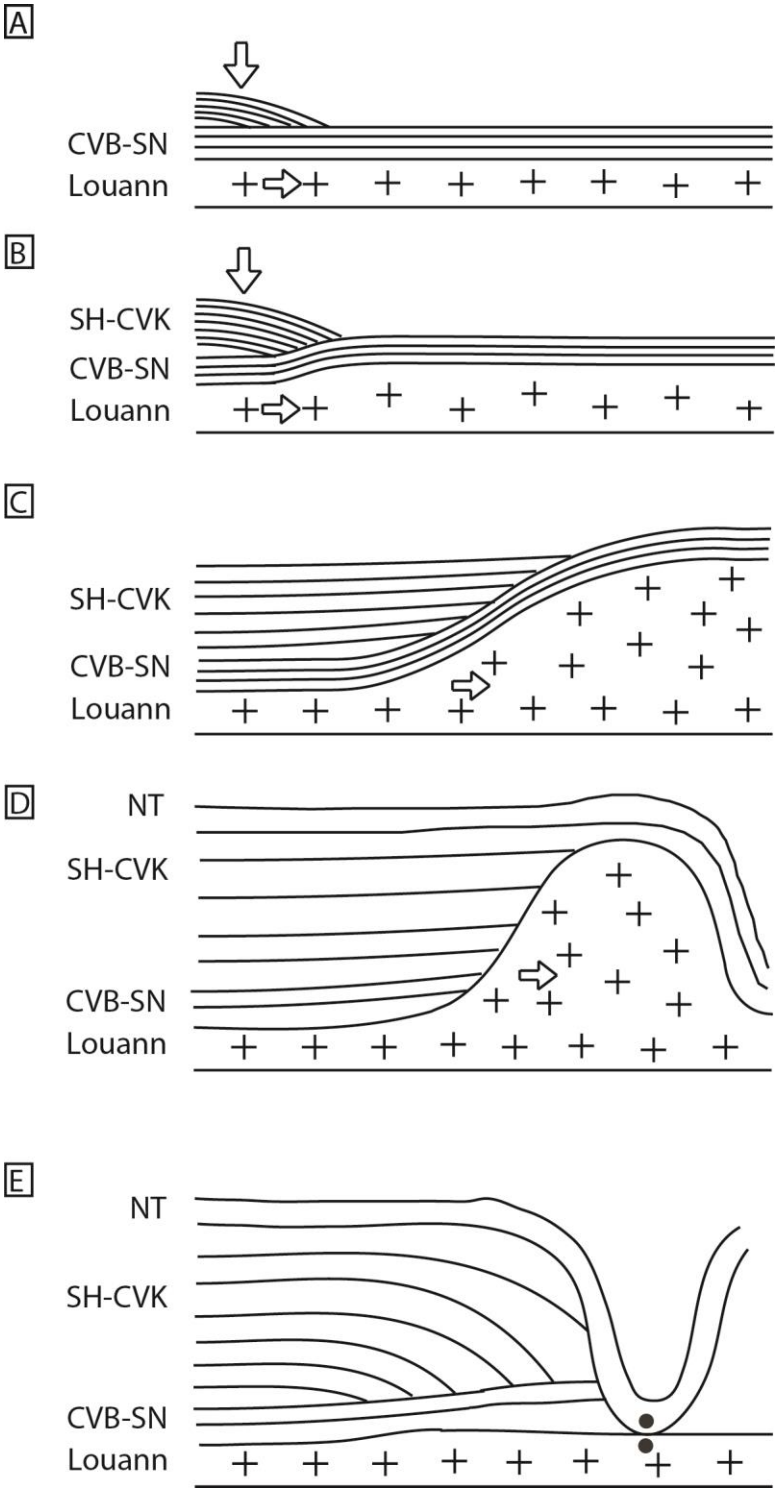

Figure 11: Schematic evolution of an asymmetric expulsion rollover, shown with units corresponding to this study. (Modified from Hudec, pers. comm.).

Chapter 2: Methodology and Data

SEISMIC DATA MAPPING

Depth-imaged 2D seismic survey lines provided to the GBDS project by Fugro were used alongside the GBDS well log, formation top, and biostratigraphy database to interpret a chronostratigraphic surface of the top of the Valanginian-Hauterivian aged-deposits across the Florida shelf, north of the Sarasota Arch, as well as the lower slope of the toe of the Florida Escarpment slope and deep-water as far west as the Mississippi Canyon protraction block.

The seismic correlation of the top of the Valanginian-Hauterivian on 2D seismic data was based on the Minerals Management Service (now BOEM) Valanginian biostratigraphy pick in the ExxonMobil EL 915 well. The Deep East 424 seismic line served as a hero line upon which the remainder of interpretations of the top of the Valanginian-Hauterivian on the shelf were based (Figure 12). Although the seismic properties of the chronostratigraphic surface vary across the shelf, the seismic and log character of the ExxonMobil EL 915 well can be compared. The Hosston reflections are usually dim (low amplitude) yet continuous, compared with the overlying Sligo reflections which are strong (higher amplitude) and continuous. This general relationship served as a guide to mapping the top of the Hosston throughout the shelf, deep-water, and Florida Escarpment slope.

Correlations could not easily be carried over the edge of the Florida Escarpment and onto the toe of the slope. Thus, MC Revival Kirchhoff, a depth-imaged, narrow azimuth (NAZ) 3D seismic survey over DeSoto Canyon and Mississippi Canyon protraction blocks, with horizon tops from biostratigraphy, was used to tie in to the 2D survey lines in the deep-water. From this new interpretation within the basin, the toe of the slope was approached and the deposits there interpreted.

The depth-imaged NAZ 3D seismic survey provided by TGS to GBDS for this study was used in the Mississippi Canyon protraction block to continue the interpretation of the chronostratigraphic Valanginian-Hauterivian top and test the hypothesis that the asymmetric expulsion rollovers are coeval to the Valanginian-Hauterivian and characterize the paleogeography of the Valanginian-Hauterivian deposits. The correlations from the 3D seismic survey to the 2D seismic survey were also used to differentiate the seismic facies of the Valanginian-Hauterivian deposits and create a seismic facies map.

Halliburton Landmark DecisionSpace seismic interpretation software was utilized to interpret the 2D and 3D seismic data, integrated with GBDS-digitized well logs and tops. Top Hosston structural and isochore maps were also created in DecisionSpace using the Frameworks to Fill module.

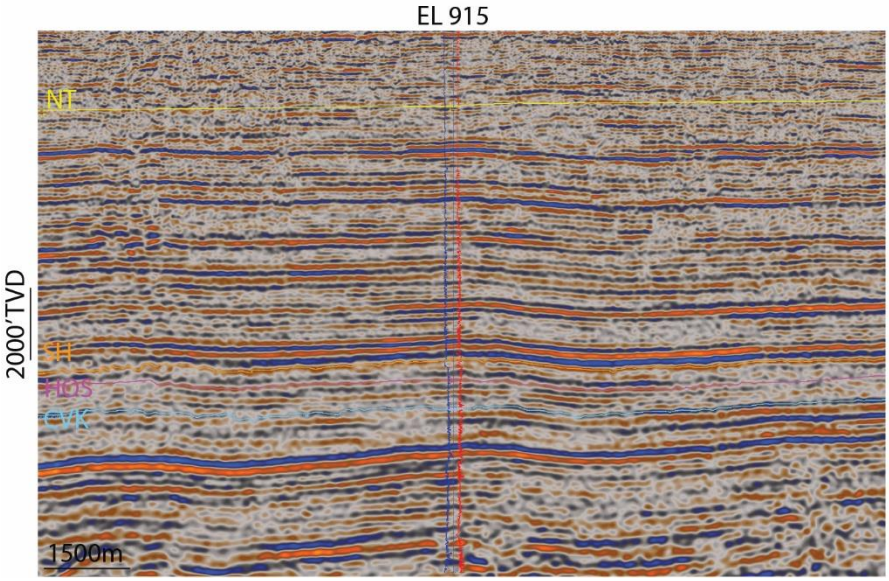

Figure 12: ExxonMobil EL 915 well with Top Cretaceous (yellow), Top Sligo (orange), Top Hosston (pink), Top Cotton Valley Knowles (blue) indicated on the log and 2D seismic. Seismic courtesy Fugro.

GRAIN SIZE ANALYSIS AND CORE DESCRIPTIONS

Grain size analysis is limited to samples obtained from one onshore well in the hypothesized bed-load dominated fluvial depositional environment of the peninsular Florida-sourced progradational sandy delta-fed apron of interest; no wells have penetrated the Valanginian-Hauterivian in the region where we predict the apron. However, this proximal well allows us to make important source-to-sink distinctions for the Valanginian-Hauterivian time, beginning with grain size analysis and core descriptions. The Stanolind-Sun Perpetual Forest #1 well, drilled in Dixie County, Florida, is representative of the hypothesized peninsular Florida-fed delta system (Figure 13).

The Florida Geological Survey maintains core cuttings (mainly unconsolidated sands) and sidewall cores from the Stanolind-Sun Perpetual Forest #1 well. Samples from each 10-foot interval were examined and the average grain size for each sample was obtained. From these observations, a grain size distribution was calculated in Excel and a weathering profile core log drawn in Adobe Illustrator.

Whole cores from the Mississippi Canyon Valanginian-Hauterivian wells have not, to the author's knowledge, been obtained and could serve as future work once available for study, in order to compare and contrast with the findings from the Stanolind-Sun Perpetual Forest #1 well studied here.

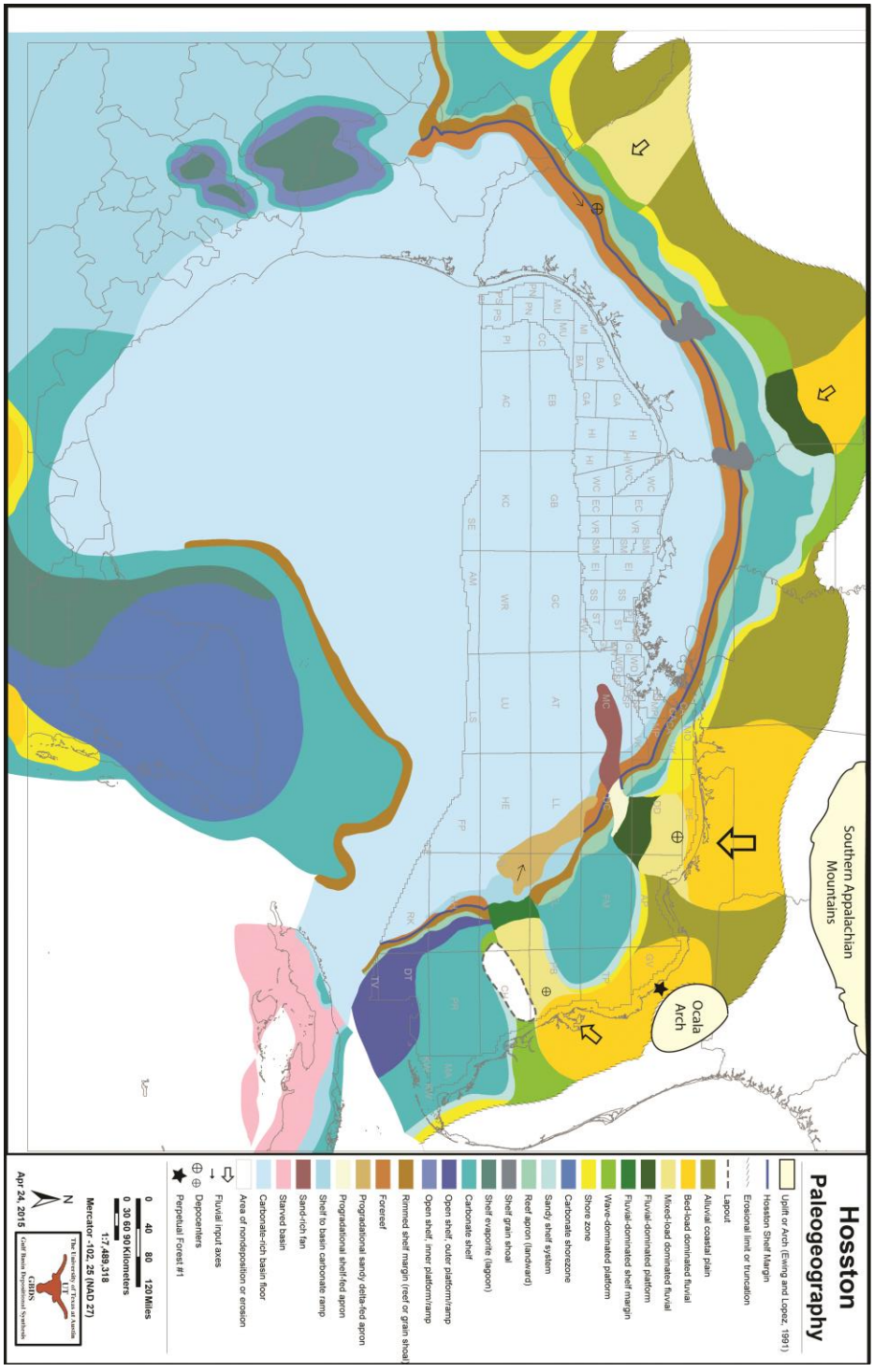

Figure 13: Hypothesized paleogeography of the Gulf of Mexico during the Valanginian-Hauterivian Hosston time. Stanolind-Sun Perpetual Forest #1 well indicated by black star. (Modified from Snedden, GBDS Phase IX).

SOURCE-TO-SINK ANALYSIS

Detrital Zircon U-Pb Analysis

Per Florida Geological Survey (FGS) regulations, less than 25% of each core cutting, chip, or core was sampled for U-Pb detrital zircon analysis. Due to limited material remaining for the Stanolind-Sun Perpetual Forest #1 well 500 g were sampled from the Valanginian-early Hauterivian section. The samples were each amalgamated from 10-foot intervals within the Hosston Formation, concentrating on the most sand-rich intervals.

The Stanolind-Sun Perpetual Forest #1 well samples were divided into an upper and lower half for a total of two samples to be processed for U-Pb detrital zircon analysis, in order to maximize the potential to capture some tectonic change with the analysis. The two samples were first crushed in order to obtain uniformly-sized grains. Next, the light and heavy minerals were separated by water on a Gemini water table and then by Broma chemical separation. Magnetic minerals were separated in a Frantz magnetizer, until 120 zircon crystals could be identified and separated by a microscope. Each of the 120 zircon crystals were then epoxied to a dish in preparation for laser ablation. Laser ablation identifies each zircon crystal separately and allows the scientist to number each crystal before performing ICP-MS analysis. The crystallization age of each zircon was then determined through ICP-MS analysis and the distribution of the age populations created. The age populations for each sample were then compared to known ages of orogenies and matched to tectonic events, leading to a determination of the source terrane from which the sedimentary deposits, including the detrital zircons, derived.

Fan Runout Length Prediction

ArcGIS ArcMap 10.1 was utilized to calculate the length of the longest river channel and fan and apron length for the progradational sandy delta-fed apron and sandy

fan. These parameters were plotted against Somme et al.'s (2009) global database of modern river and fan systems to compare the results of the seismic mapping to what can be expected for source-to-sink systems world-wide.

Using the line measure tool in ArcMap, an average river length, defined as the length from the headwaters to the shelf edge, was calculated from five potential pathways for the peninsular Florida-fed source to sink system. The five potential pathways and average river length model a paleo-Suwannee River whose headwaters lay in the Ocala Arch.

The line measure tool in ArcMap was also used to calculate an average river length of five potential pathways for the Appalachian-fed source-to-sink system. The five potential pathways and average river length model a paleo-Chattahoochee-Apalachicola River. The average river length was then compared to five potential pathways of the modern Chattahoochee-Apalachicola River, calculated from modern river length (Couch et al., 1996) and five potential pathways from river mouth to shelf edge, using the line measure tool in ArcGIS (Figure 14). A third method for determining the river length of the Appalachian-fed system was considered using the North American drainage basin extent for the Gulf of Mexico of the early Cretaceous defined by Blum and Pecha (2014; Figure 15). The river channel length in this third model was extended north to the drainage basin divide as a high-end estimate.

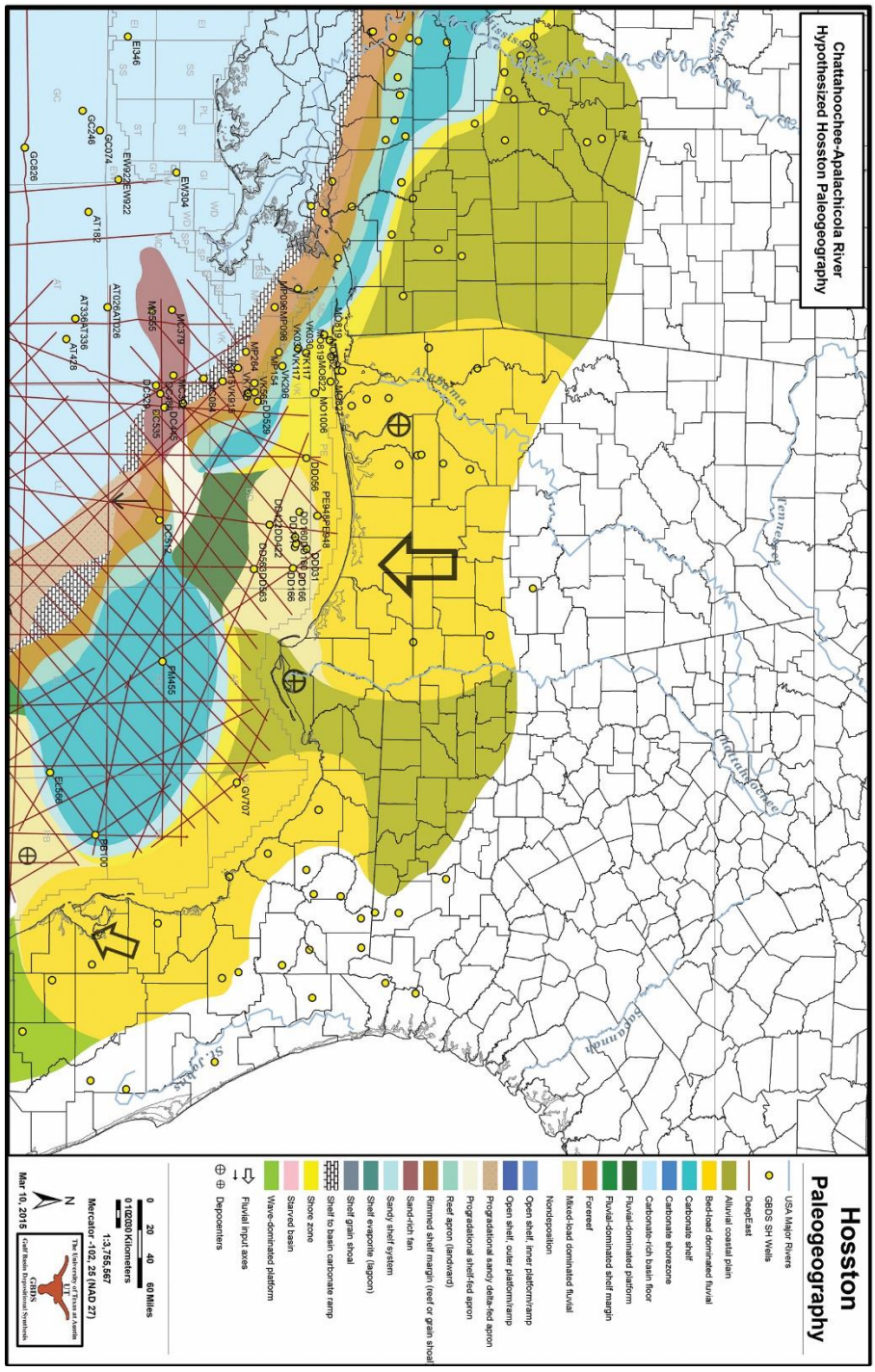

Figure 14: Modern Chattahoochee-Apalachicola River pathway shown on hypothesized Hosston Paleogeography map to illustrate one method considered in determining the river channel length in order to predict fan length in the Somme et al. (2009) method.

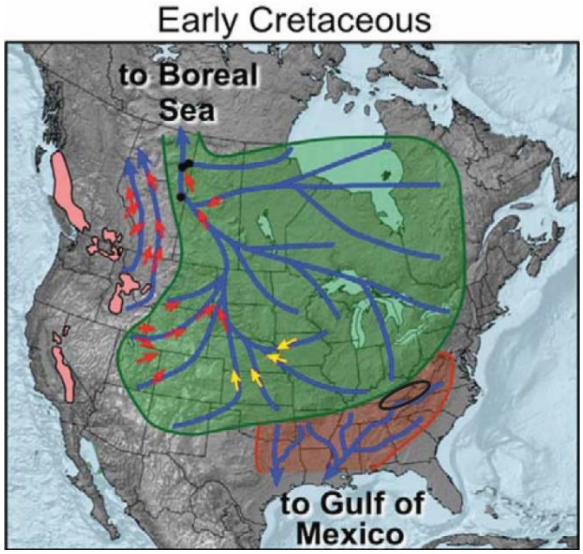

Figure 15: Early Cretaceous North American drainage basin reorganization based on detrital zircon analysis. The southern Appalachian Mountains sourced Gulf of Mexico deposition while the northern Appalachian Mountains and the Rocky Mountains sourced Boreal Sea deposition. Black oval indicates region from which the longest river channel length was measured in the third method of determining the river channel length of the Appalachian-sourced system in this study. Note "locations of fluvial axes are schematic." (Modified from Blum and Pecha, 2014).

NEW HOSSTON PALEOGEOGRAPHIC MAP

ArcGIS ArcMap 10.1 was utilized to update the Hosston paleogeographic map first created by the GBDS team in 2013. Individual polygons for the paleogeographic features were edited according to the seismic interpretation.

Chapter 3: Results

SEISMIC MAPPING

Florida Shelf

Mapping on the modern Florida shelf indicates a 2D seismically-defined boundary between the Hosston and overlying Sligo does indeed exist. It is defined in this study as the last trough between the continuous, acoustically fast Sligo carbonates and the sometimes discontinuous, weak, acoustically slower Hosston siliciclastics underneath (Figure 16).

Clinoforms are found to be preserved in the Hosston on the modern Florida shelf (Figure 17). The average clinoform height determined from clinoforms found on four 2D seismic lines is about 100 m. Clinoforms of this scale are considered to be shelf-prism scale (Patruno et al., 2015).

Florida Escarpment Slope

The Hosston can be mapped in the deep-water of the Mississippi Canyon and DeSoto Canyon protraction blocks and traced back to the slope of the Florida Escarpment. At the lower slope of the toe of the slope are Hosston sediments of dim, (low amplitude reflections. This apron, or base-of-slope apron as termed by Mullins and Cook (1986), represents the terminus of the Valanginian-Hauterivian Hosston deposition off the Florida Escarpment. GBDS classifies this apron as a sandy progradational delta-fed apron.

Eastern Gulf of Mexico Deep-water

The seismic character of the Hosston changes in the deep-water, from the high-to-moderate-continuity, high-to-moderate-amplitude character on the shelf to low-continuity, low amplitude character. The extent of the Hosston slow reflections in DeSoto Canyon and

Mississippi Canyon is mapped in Figure 18, and is termed the dim seismic facies, representing siliciclastic Valanginian-Hauterivian material.

3D seismic reveals features in Mississippi Canyon poorly imaged on 2D seismic available to GBDS. It is found that the deposition coincident with the development of asymmetric expulsion rollovers includes the Hosston Valanginian-Hauterivian time, extending from Cotton Valley-Bossier Tithonian time to Navarro-Taylor Campanian-Maastrichtian time (Figure 19). The Appomattox well, MC 392 #1, reveals 49 m of Valanginian-Hauterivian material, compared with the 335 m of carbonate material in the updip Shiloh (DC 269 #1) well (Figure 20).

The asymmetric expulsion rollovers, which we believe preserve the direction of sediment input, indicate the Hosston was deposited from the ENE to a WSW terminus. This ENE-WSW depositional direction supports the hypothesis that the Valanginian-Hauterivian fan of Mississippi Canyon was fed by a delta generated by an Appalachian river, not a paleo-Mississippi River.

Structure maps of the Top Hosston and Top Cotton Valley Knowles surfaces were constructed using the Frameworks to Fill module in Landmark DecisionSpace. The structure map of the Top Hosston reveals a relatively gentle sloped shelf , which dips down in depth northwest of the Sarasota Arch, before the surface rises and onlaps onto the structural high (Figure 21). The structure map reflects the geometry of the paleo-shelf edge. The isochore map reveals Hosston thickening as it approaches the shelf edge, and areas of thinning in the deep-water (Figure 22).

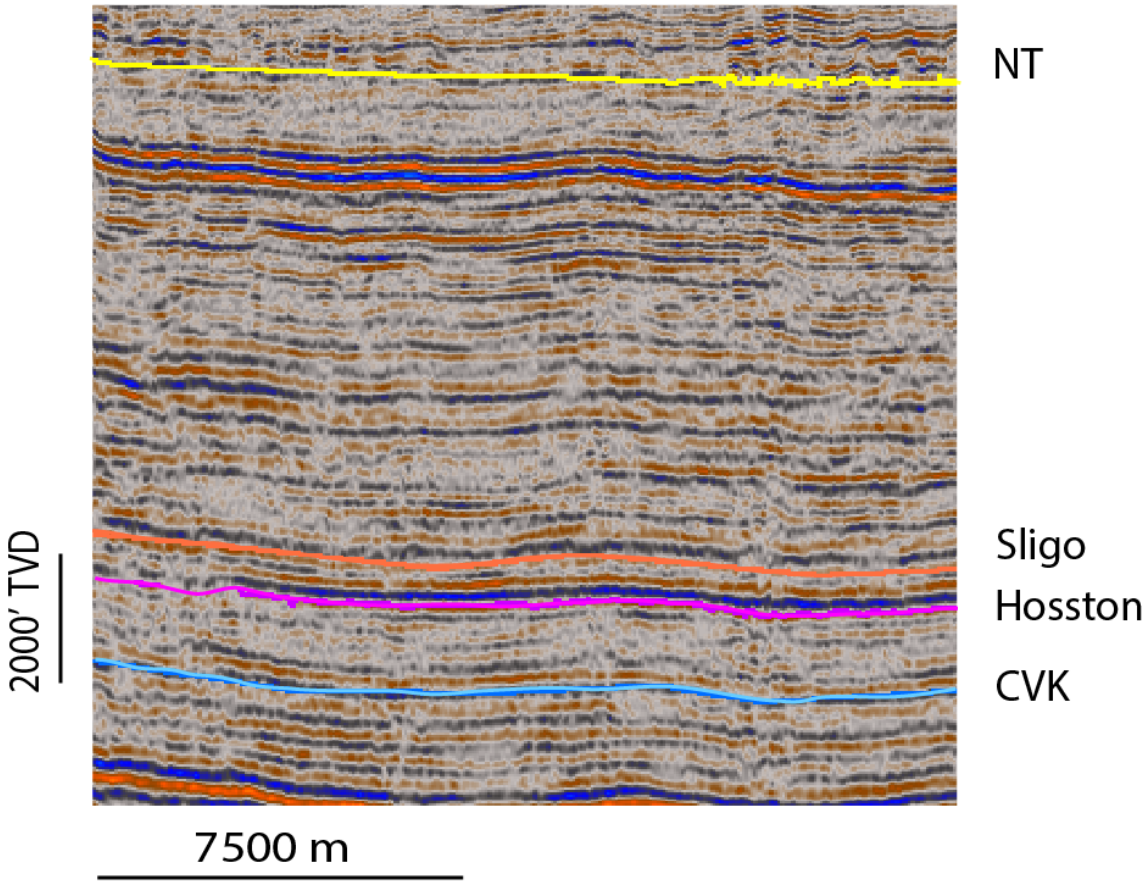

Figure 16: Representative 2D seismic character of top Hosston on Florida shelf. Continuous, hard, fast, strong-amplitude Sligo carbonates overlying discontinuous, slower, weaker amplitude Hosston siliciclastics. Top Hosston marked in pink. Top Cretaceous included for reference. Seismic data courtesy Fugro.

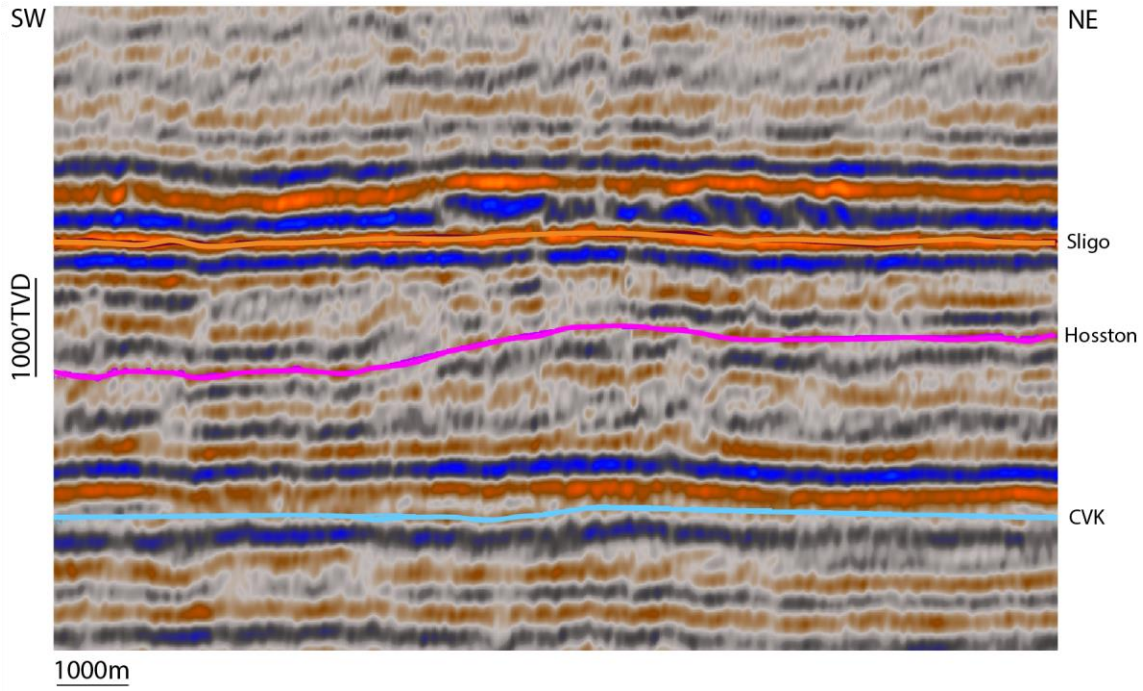

Figure 17: 2D seismic line displaying shelf-prism-scale clinoforms found within the Hosston (pink). Top Sligo (orange) and top Cotton Valley Knowles (blue) are also interpreted. Seismic data courtesy Fugro.

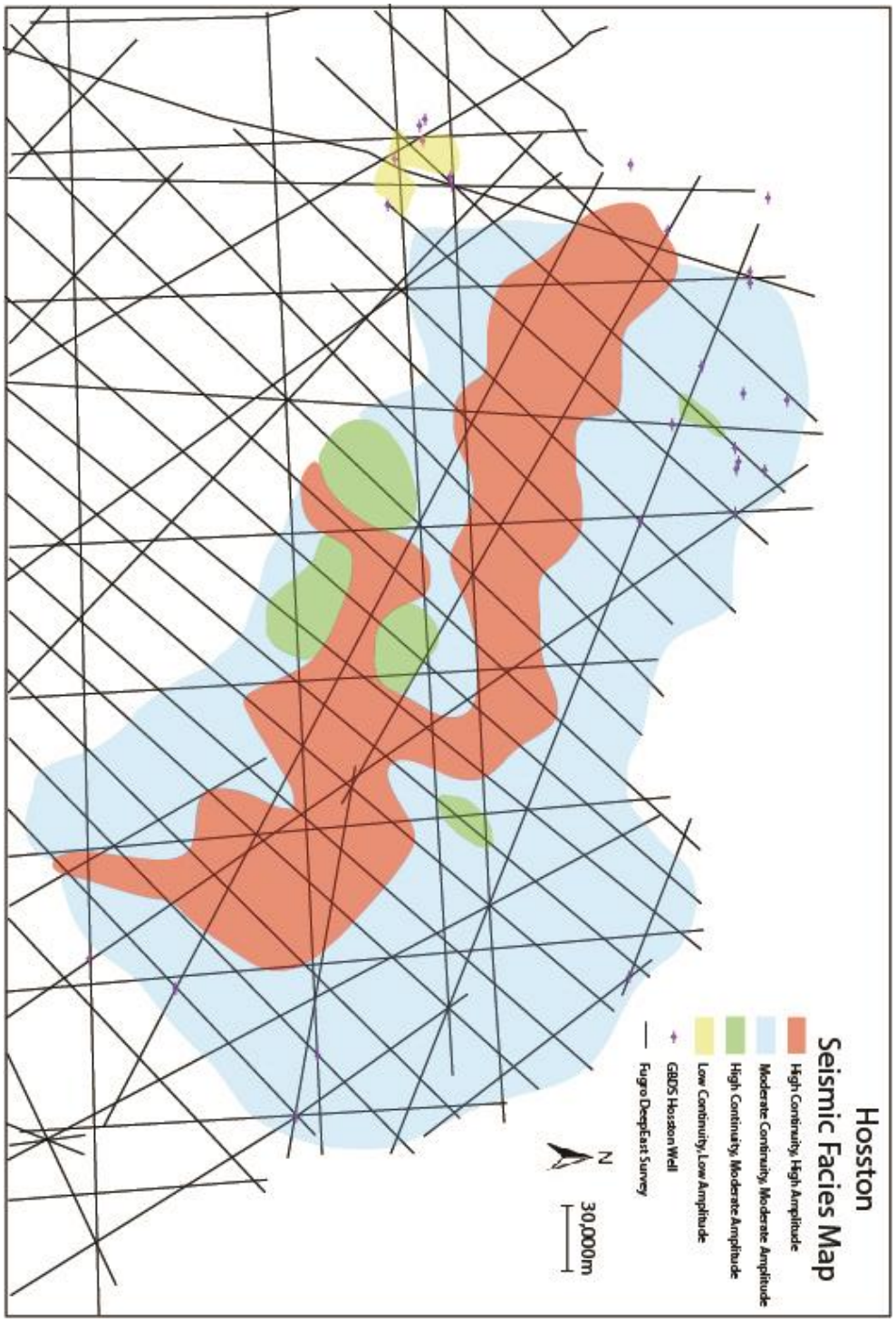

Figure 18: Seismic facies map of the Valanginian-Hauterivian Hosston formation, highlighting the dim seismic facies, interpreted to be the extent of the siliciclastic deposition of the Appalachian-sourced depositional system.

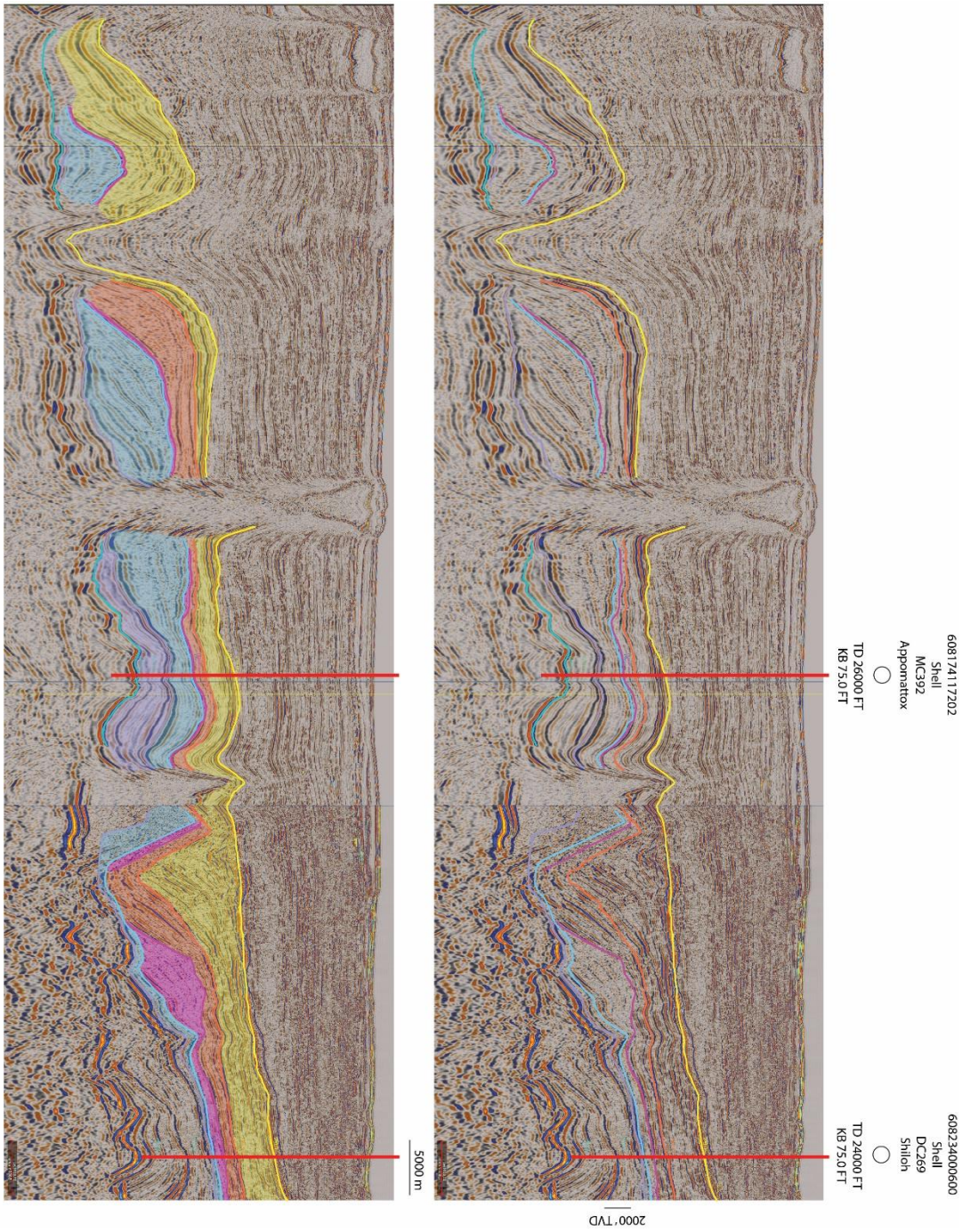

Figure 19: Asymmetric expulsion rollover in Mississippi Canyon. Top Navarro-Taylor (yellow), Top Sligo (orange), Top Hosston (pink), Top Cotton Valley Knowles (blue), Top Cotton Valley Bossier (purple), Top Smackover (teal). Interpretations based on tops in DC 269 and MC 392 #2 wells. 3D Seismic data courtesy TGS and 2D seismic data courtesy Fugro.

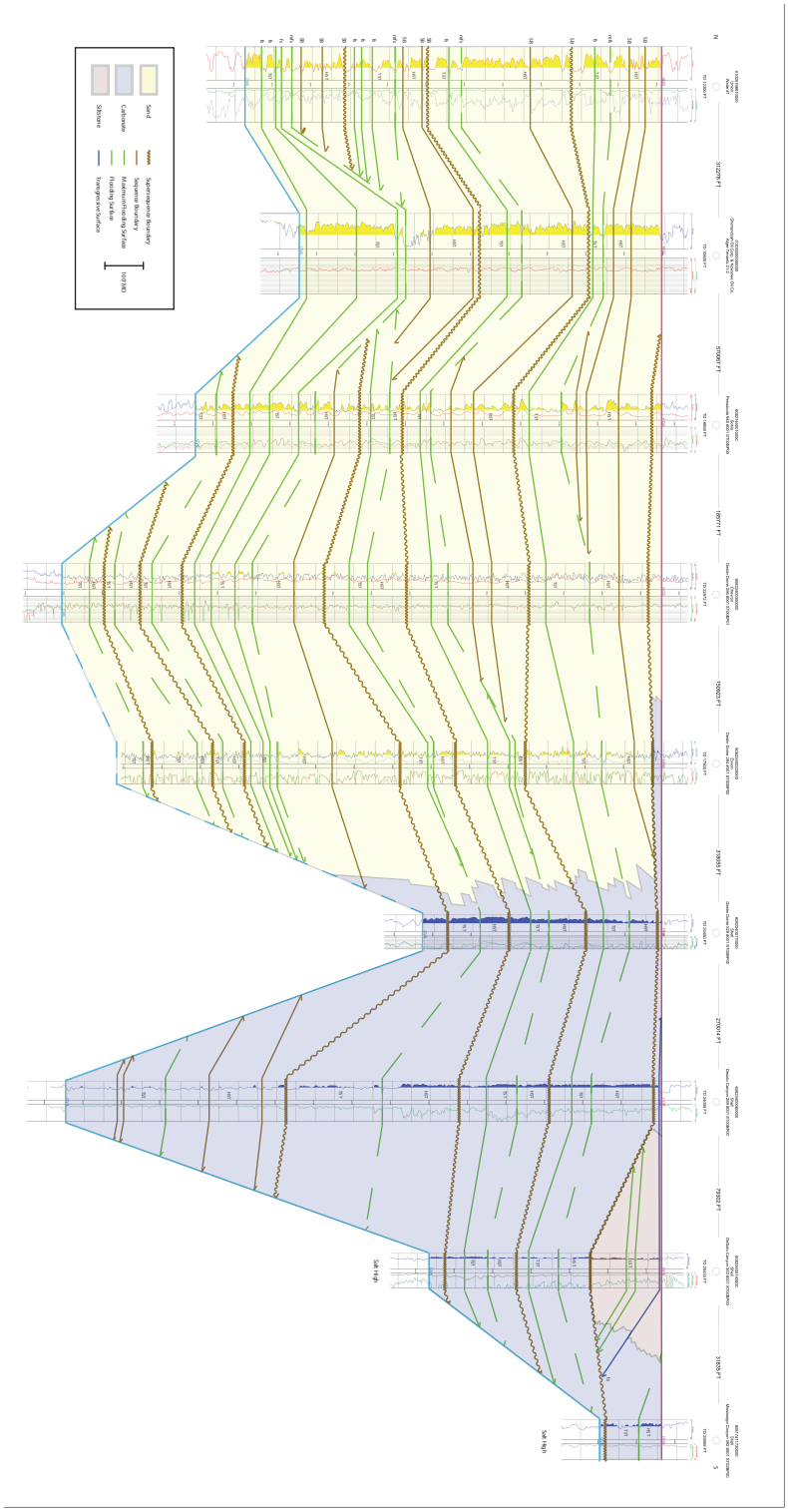
Sand
Carbonate
Siltstone
Sequence Boundary
Maximum Flooding Surface
Transgressive Surface
1107 MD
Salt High
Salt High
N
S

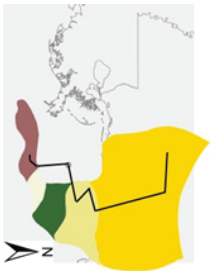
N

Figure 20.

Figure 20: N-S onshore to offshore Hosston stratigraphic cross section, hung on Top Hosston, base Top Cotton Valley Knowles. Orientation shown on location map. Sequence stratigraphic surfaces interpreted. Note lowstand wedge interpreted pinching out just basinward of the DC 353 Vicksburg B well (see Figure 19 for fan location in seismic).

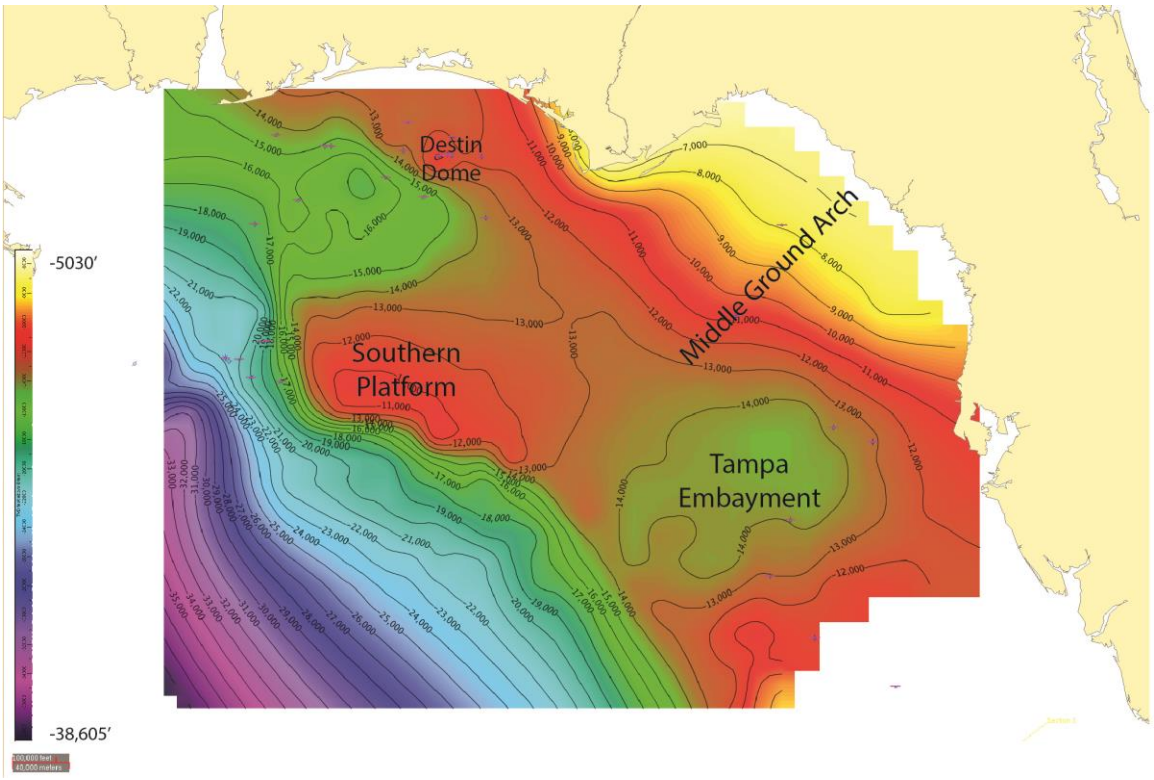

Figure 21: Structure map of the top of the Hosston Formation over the eastern Gulf of Mexico. 1000 ft contours.

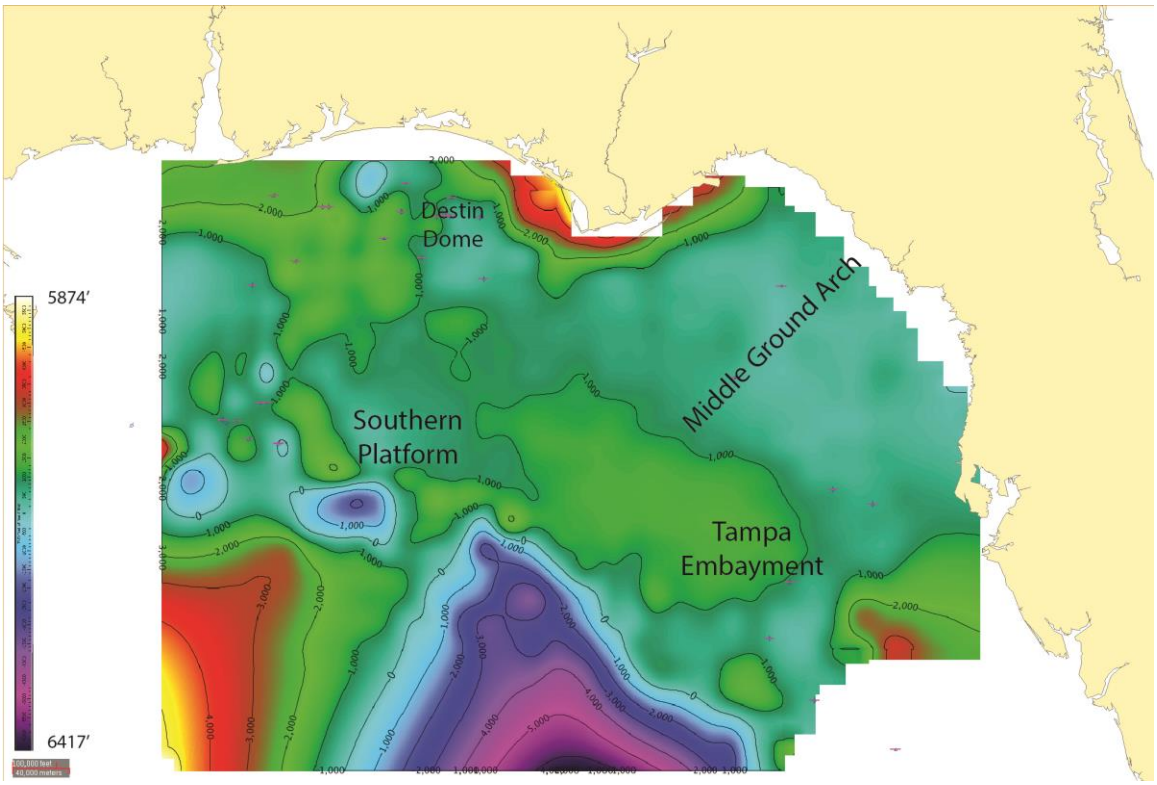

Figure 22: Isochore map of the top of the Hosston to the top of the Cotton Valley Knowles over the eastern Gulf of Mexico. 1000 ft contours.

WELL LOG CORRELATION

Correlation of well logs in a stratigraphic dip section from onshore Alabama to the deep-water of Mississippi Canyon allows for conclusions to be made about the hypothesized Appalachian-sourced depositional system (Figure 20). Multiple stacked transgressive and highstand systems tracts are interpreted across the onshore-to-offshore Hosston section. Many of the maximum flooding surfaces and sequence boundaries extend across the entire section, through changing lithologies. Beginning with Union Waite #1 and Shenandoah Oil/Kewanee Oil Alger-Tenants #1 wells, the Valanginian-Hauterivian section represents bed load-dominated fluvial deposits. Moving downdip to Sohio PE 948 #1, the Hosston transitions to a mixed load-dominated fluvial shelf depositional

environment, before the shore zone encountered by the Chevron DD 56 #1 well. Exxon DD 284 #1 contains the first carbonate lithology in the Hosston at the top of the section, underlain by mixed load-dominated shelf deposits. The Hosston rimmed shelf margin reef is penetrated by the Shell DD 529 #1 well and is the first all-carbonate well of this dip cross section. Shell DC 269 #1 encounters the fore reef and Shell DC 353 #1 captures the distal fore reef carbonates, as well as a siltstone lowstand fan interpreted from depths 20,120 ft MD – 20,300 ft MD. The location of this lowstand fan is consistent with the seismic facies observed on 2D and 3D seismic data and represents the distal, mud-rich edge of the sandy fan. Shell MC 392 #1 is interpreted to be beyond the extent of the sandy, lowstand fan as the Valanginian-Hauterivian interval is of a carbonate lithology.

GRAIN SIZE ANALYSIS AND CORE DESCRIPTIONS

Grain size of the Hosston formation in the Stanolind-Sun Perpetual Forest #1 well ranges from fine-to coarse-grained sand (Figure 23). 49% of the observed samples were found to be medium-grained, 27% of the observed samples were found to be coarse-grained, 16% fine-grained, and 7% coarse-grained.

The coarse- and very coarse-grained sands found in the Stanolind-Sun Perpetual Forest #1 well could suggest that the Hosston sands are in relatively close proximity to their source. The medium-grained sands are appropriate for the hypothesized source terrane of the Ocala Arch. If the Hosston sands found in the Stanolind-Sun Perpetual Forest #1 well were sourced by an Appalachian terrane instead of the peninsular Florida terrane, a distribution with greater percentage of grains in the fine to medium range would be expected, due to progressive sorting (Russell, 1939).

The core and cuttings of the Hosston interval of the Stanolind-Sun Perpetual Forest #1 well are mainly comprised of light yellow to white to clear sand, with some intercalated

beds of red sand and red mud (red beds), indicative of an alluvial settings (Turner, 1948; Figure 24).

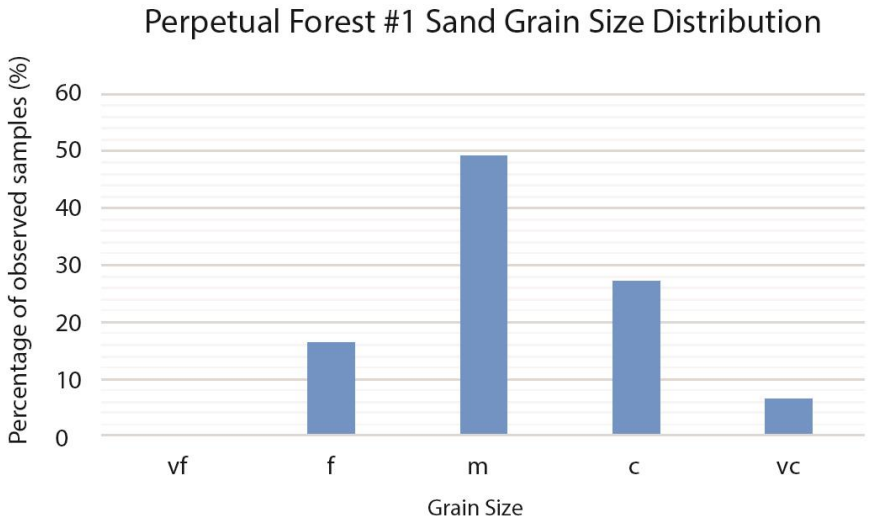

Figure 23: Grain size analysis of the Hosston interval of the Stanolind-Sun Perpetual Forest #1.

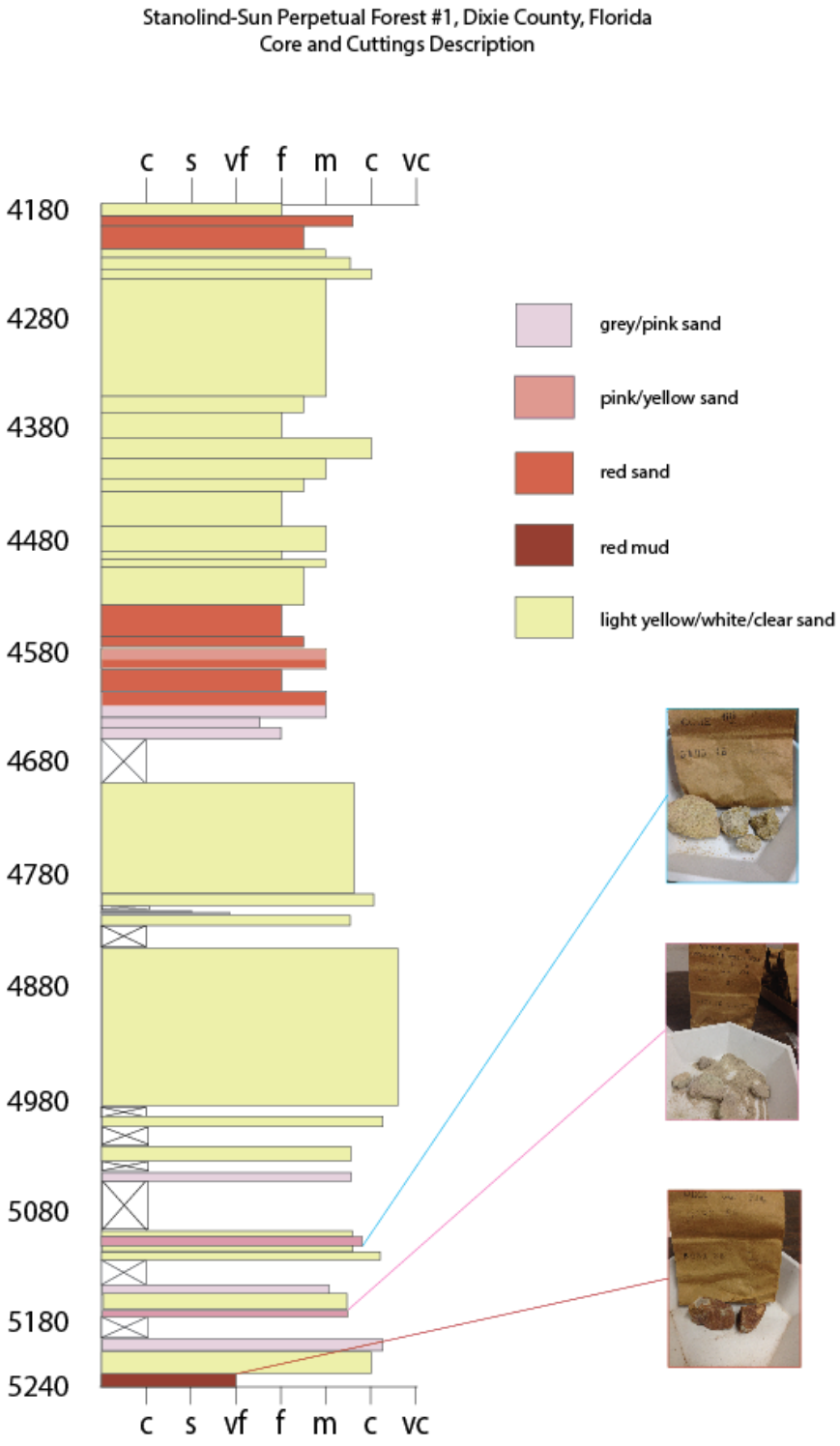

Figure 24: Weathering profile core description log of the Hosston interval of the Stanolind-Sun Perpetual Forest #1 well.

DETRITAL ZIRCON U-PB DATING

U-Pb detrital zircon analysis of the upper half (4180–4700ft MD) of the Hosston interval of the Stanolind-Sun Perpetual Forest #1 well reveals two basement source terrane age populations: 493-699 Ma and 1992-2240 Ma (Figure 25).

U-Pb detrital zircon analysis of the lower half (4700–5230ft MD) of the Hosston interval of the Stanolind-Sun Perpetual Forest #1 well reveals two roughly similar age populations: 514-697 Ma and 2050-2168 Ma (Figure 26).

While two main age populations are found for the two samples, outlier U-Pb ages are evident, including five of 118 zircons of the upper half of the Stanolind-Sun Perpetual Forest #1 with ages corresponding with the Grenvillian basement province (1039-1260 Ma). Similarly, three of the 110 zircons of the lower half of the Stanolind-Sun Perpetual Forest #1 have ages corresponding with the Grenvillian basement province (1022-1161 Ma).

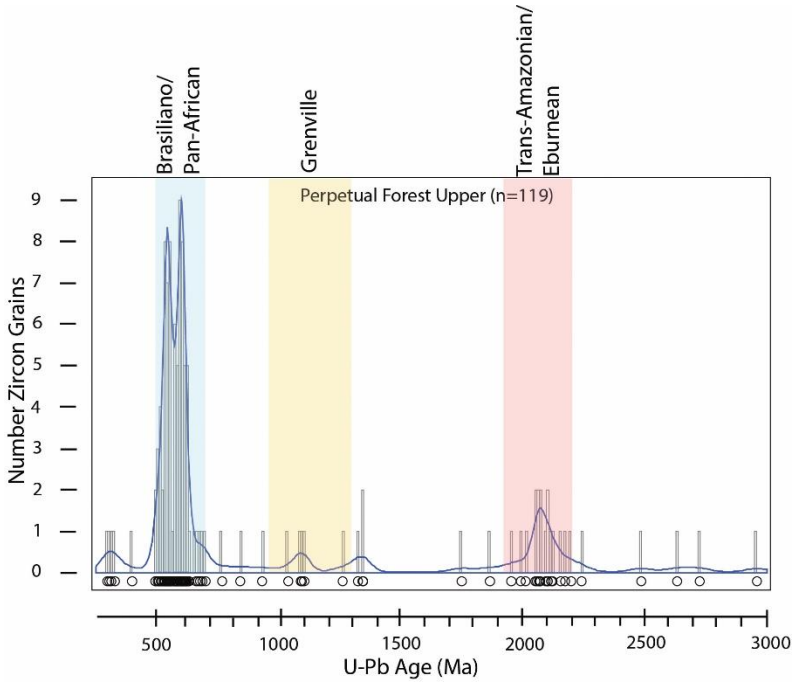

Figure 25: U-Pb detrital zircon age populations of Stanolind-Sun Perpetual Forest #1 upper half sample (4180–4700ft MD).

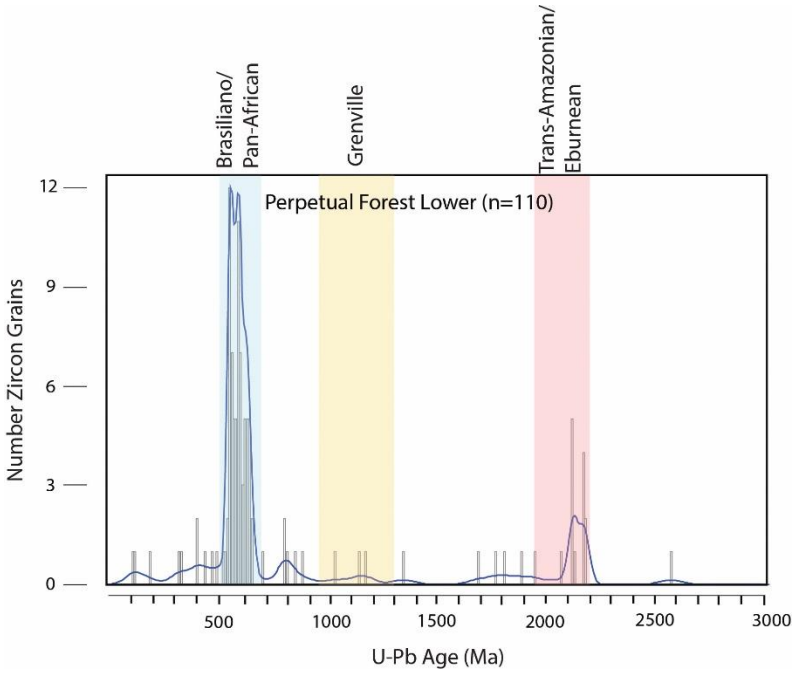

Figure 26: U-Pb detrital zircon age populations of Stanolind-Sun Perpetual Forest #1 lower half sample (4700–5230ft MD).

FAN RUNOUT LENGTH PREDICTION

Using the line measure tool in ArcGIS, an average river length of the Florida-sourced Hosston source to sink system was calculated from five potential pathways. Distance from the interpreted headwaters to shelf edge, is approximately 400-462 km, with an average of 424 km (Table 1). If Somme et al.'s (2009) empirical scaling relationships between river channel length and fan length are applied to the Hosston apron, the relationship can help us place seismic observations into a better context. The paleo-Suwannee River channel average length of 424 km would scale with an apron approximating 10-50% the length of the river channel (Somme et al., 2009; Figure 9), predicting an apron of 42-212 km length (Table 2). The mapped apron of the Florida-sourced system is 200 km-long, at the long end of the distribution but within the predicted range. Certainly there is potential for the estimated longest river length to be much shorter.

Using the line measure tool in ArcGIS, an average river length of the Appalachian-sourced Hosston source to sink system, defined as the length from the headwaters to the shelf edge, calculated from five potential pathways, is 887 km (Table 2). This average river length is much shorter than the same pathway drawn following the exact path of the modern Chattahoochee-Apalachicola fluvial system (1107 km; Table 2). An average river length of 1349 km derived from the schematic map of Blum and Pecha (2014) showing an early Cretaceous drainage divide, which represents the longest pathway that could be considered for this system (Table 2).

The paleo-Chattahoochee-Apalachicola River channel length of 887 km, when expected to yield a fan of 10-50% the length of the longest river channel (Somme et al., 2009; Figure 9), would yield a fan of 89-443 km length (Table 2). This compares with the modern Chattahoochee-Apalachicola River channel length of 1107 km, which would yield a fan of 111-553 km length (Table 2). The longest river channel extending to the drainage

divide defined by Blum and Pecha (2014), 1349 km in length, would yield an expected fan length of 135-674 km (Table 2). The mapped fan of the Appalachian-sourced system, using seismic data alone, is approximately 70 km-long. This is shorter than most of the empirical predictions but may reflect the complexity of salt-influenced depocenters and enhanced accommodation which may limit fan runout distance. Like the paleo-Suwannee River, there is potential for the longest river length of the paleo-Chattahoochee-Apalachicola River to be much shorter.

	River Channel Length (km)	Expected Apron Length Range (km)
Paleo-Suwannee River 1	401	
Paleo-Suwannee River 2	411	
Paleo-Suwannee River 3	440	
Paleo-Suwannee River 4	462	
Paleo-Suwannee River 5	406	
Average	424	42 – 212

Table 1: River transect lengths used to calculate expected progradational sandy delta-fed apron length range, based on Somme et al.'s (2009) relationship: fan lengths are 10-50% of the river length. River length includes the straight distance from the river mouth to the shelf break, in addition to the path over land. Paleo-Suwannee River paths approximated from approximate center of Ocala Arch.

	River Channel Length (km)	Expected Fan Length Range (km)
Paleo-Chattahoochee-Apalachicola 1	898	
Paleo-Chattahoochee-Apalachicola 2	893	
Paleo-Chattahoochee-Apalachicola 3	859	
Paleo-Chattahoochee-Apalachicola 4	909	
Paleo-Chattahoochee-Apalachicola 5	875	
Average	887	89 – 443
Modern Chattahoochee-Apalachicola 1	1094	
Modern Chattahoochee-Apalachicola 2	1132	
Modern Chattahoochee-Apalachicola 3	1102	
Modern Chattahoochee-Apalachicola 4	1103	
Modern Chattahoochee-Apalachicola 5	1103	
Average	1107	111-553
Drainage Divide Chattahoochee-Apalachicola 1	1353	
Drainage Divide Chattahoochee-Apalachicola 2	1277	
Drainage Divide Chattahoochee-Apalachicola 3	1407	
Drainage Divide Chattahoochee-Apalachicola 4	1385	
Drainage Divide Chattahoochee-Apalachicola 5	1322	
Average	1349	135-674

Table 2: River transect lengths used to calculate expected fan length range, based on Somme et al.'s (2009) relationship: fan lengths are 10-50% of the river length. River length includes the straight distance from the river mouth to the shelf break, in addition to the path over land. Paleo-Chattahoochee-Apalachicola river paths approximated from approximate location of modern headwaters.

NEW HOSSTON PALEOGEOGRAPHIC MAP

ArcGIS 10.1 was utilized to update the Hosston paleogeographic map first created by the GBDS team in 2013 (Figure 27). Individual polygons for the paleogeographic features were edited according to the seismic interpretation, resulting in a shorter sandy fan in Mississippi Canyon, and a progradational sandy delta-fed apron shorter in axial distance.

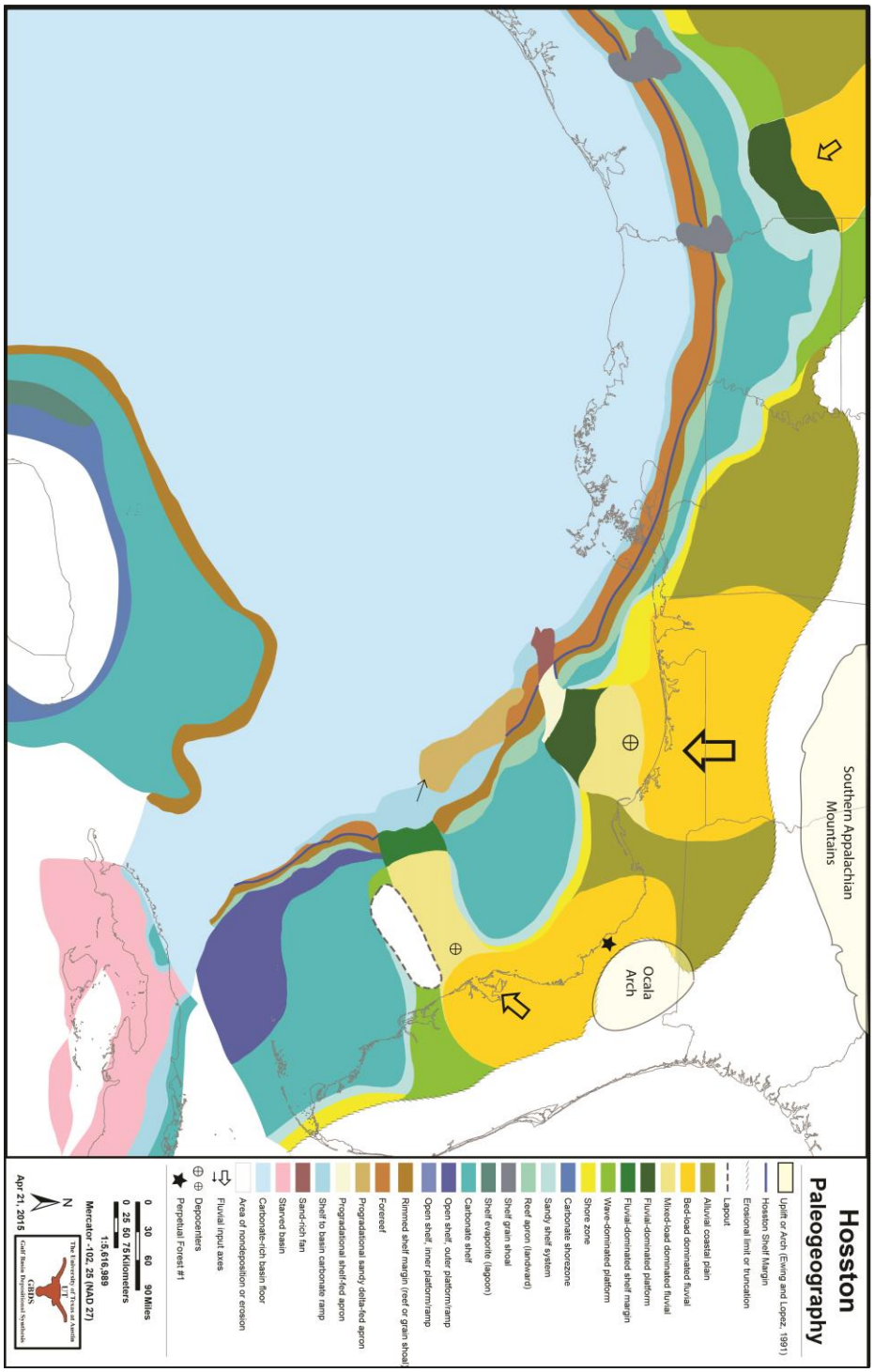

Figure 27: New Hosston paleogeographic map developed based on the results of this study. Note smaller progradational sandy delta-fed apron and smaller sandy fan in Mississippi Canyon compared with hypothesized map.

Chapter 4: Discussion

TECTONICS

Full consensus on the timing of initiation of sea-floor spreading in the GOM remains to be achieved (Hudec et al., 2013). Yet new seismic reflection and refraction data yield convincing evidence for the termination of sea-floor spreading in the Valanginian time (133 – 138 Ma; Snedden et al., 2013). The extinct spreading center crosses the present-day Lund protraction block and continues to the northwest (Snedden et al., 2014). It is possible that structural reorganization followed the end of GOM sea-floor spreading, including uplift of the Florida Peninsular Arch and its northern extension, the Ocala Arch in present north central Florida. The Ocala arch is located over what had been the Suwannee Basin in the early Jurassic (Ewing and Lopez, 1991). With termination of sea-floor spreading in the Valanginian, orogenesis of the Ocala Arch was also likely to have ceased, and the perched Ocala Arch was primed as a source terrane for eroding sediments. The end of sea floor spreading was followed by a similar tectonic reorganization and uplift in the Oligocene-Miocene time in the Labrador Sea (Tsikalas et al., 2012).

The hypothesized Valanginian-Hauterivian-aged progradational sandy fan located in Mississippi Canyon is north of the GOM spreading center, and thus more structurally influenced by local salt tectonics. Mississippi Canyon contains a diverse array of salt features, including salt welds, turtle structures, ascension zones, the autochthonous and parautochthonous salt, the allocthonous salt canopy, and asymmetric expulsion rollovers. The asymmetric expulsion rollovers, which might preserve direction of sedimentary sourcing, are found to be coeval to the Valanginian-Hauterivian Hosston deposition, and prograde in a NE-SW pattern on the east side of Mississippi Canyon (McDonnell, 2010). This suggests an Appalachian-fed delta system for the Hosston formation in the Mississippi Canyon deep-water.

BASIN ENTRY POINTS

Seismic analysis leads to the interpretation that the Valanginian-Hauterivian Hosston formation formed at the toe of the slope of the Florida Escarpment, but what transport processes allowed for the interpreted sandy apron to be deposited? A present-day analog in northeast Australia, where deposition is mixed carbonate-siliciclastic at the Great Barrier Reef margin, allows us to gain insight into the processes that contribute to siliciclastic deposition in the deep-water in a reef-rimmed basin. Puga-Bernabéu et al. (2011) analyzed high-resolution multibeam bathymetry and side-scan sonar data to characterize submarine canyons and interpret depositional processes at the Great Barrier Reef margin.

Two types of submarine canyons are observed at the modern Great Barrier Reef margin: shelf-incised canyons and slope-confined canyons (Puga-Bernabéu et al., 2011). The heads of the shelf-incised canyons are incised into the shelf-break at water depths of 60-80 m and may be reef-blocked, partially reef-blocked, or shelf-connected (Puga-Bernabéu et al., 2011). Puga-Bernabéu et al. (2011) observed deeper waters on the slope of slope-confined canyons. A four-phase development model of both submarine canyon types originally proposed by Farre et al (1983) is observed: (1) initial stage: local slope failures due to low sediment strength, underconsolidation, differential compaction, permeability, or faults triggered by earthquakes, fluid escapes, sediment overpressure, or oversteepening; (2) transition stage: slope failures continue upslope; (3) mature stage: a change in erosion style occurs in which the erosion may breach the shelf-edge, canyon heads become local catchment heads, and axial incision occurs and linked walls collapse; (4) reef-blocking stage: growth of extensive shelf-edge barrier reef, the location and morphology of which controls the type and amount of sediment supplied to the basin (Figure 28; Puga-Bernabéu et al., 2011). Puga-Bernabéu et al. (2011) conclude that

submarine canyons entirely blocked by reefs receive only the carbonate reef material has eroded into the canyon; however, partially reef-blocked submarine canyons can receive mixed carbonate and siliciclastic input, or siliciclastic dominated input (Figure 29).

Puga-Bernabéu et al. (2011) do not have seismic data available to include in their study. Additional interpretations can be made taking the concepts of submarine canyon retrogradational failure into account, along with the Great Barrier Reef model of a partially-blocked system, and applying it to the 2D seismic data imaging over the Hosston sandy apron off the Florida Escarpment. In strike view, numerous incisions are seen at the top of the Hosston (Figure 30) and such a process in which submarine canyons incised the shelf edge, bringing both the carbonate reef rim material and siliciclastic material from where open shelf passages exist, down to the deep-water. Plausible processes include debris flows, hybrid flows, and turbidity flows. Without bathymetry and side-scan sonar from the Valanginian-Hauterivian age, we cannot see each submarine canyon that brought siliciclastics to the apron, but we can imagine that the Valanginian-Hauterivian Florida Escarpment could have looked like the modern Great Barrier Reef margin as investigated by Puga-Bernabéu et al. (2011; Figure 31).

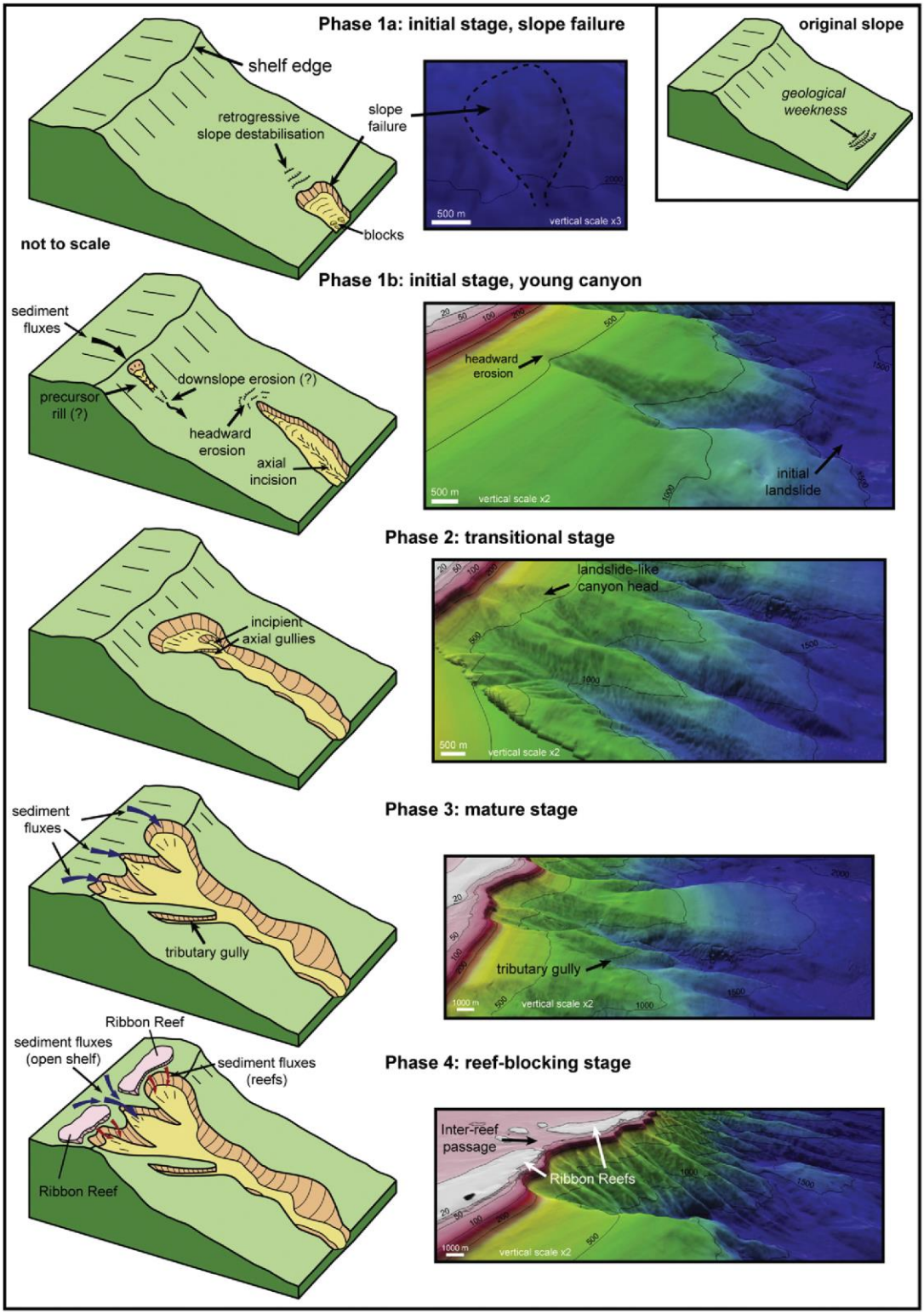
Phase 1a: initial stage, slope failure
shelf edge
retrogressive slope destabilisation
slope failure
blocks
not to scale
500 m
vertical scale x3
original slope
geological weekness
Phase 1b: initial stage, young canyon
sediment fluxes
downslope erosion (?)
precursor rill (?)
headward erosion
axial incision
headward erosion
initial landslide
500 m
vertical scale x2
Phase 2: transitional stage
incipient axial gullies
landslide-like canyon head
500 m
vertical scale x2
Phase 3: mature stage
sediment fluxes
tributary gully
tributary gully
1000 m
vertical scale x2
Ribbon Reef
sediment fluxes (open shelf)
sediment fluxes (reefs)
Ribbon Reef
Phase 4: reef-blocking stage
Inter-reef passage
Ribbon Reefs
1000 m
vertical scale x2

Figure 28.

Figure 28: Canyon development model of the Ribbon Reef region of the Great Barrier Reef, Australia, derived from morphological characteristics observed in Digital Elevation Model (DEM) sections. The outcome of the final stage, Phase 4, in which a reef may partially or fully block the canyon head, determines the type of sediments that may be deposited beyond the shelf edge and their source. (From Puga-Bernabéu et al., 2011).

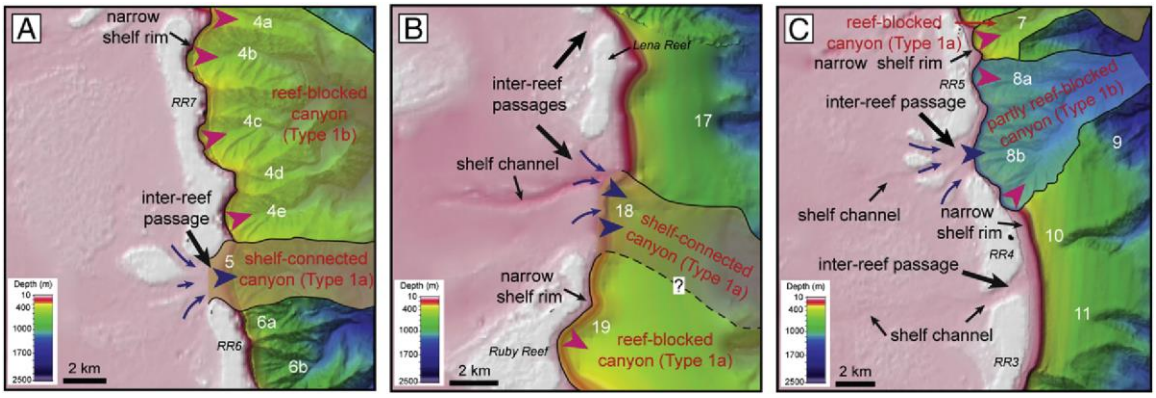

Figure 29: Examples from the Ribbon Reef region of the Great Barrier Reef, Australia of shelf-connected canyons displayed on hillshaded relief maps adjacent to reef-blocked canyons or partially reef-blocked canyons. A) Shelf-connected canyon allows for inter-reef passage of sediments, found adjacent to reef-blocked canyon in which reef-derived sediment is deposited. B) Another example of a shelf-connected canyon adjacent to a reef-blocked canyon. C) Partially reef-blocked canyon in which inter-reef passage of sediments occurs in tandem with reef-derived sedimentation. (From Puga-Bernabéu et al., 2011).

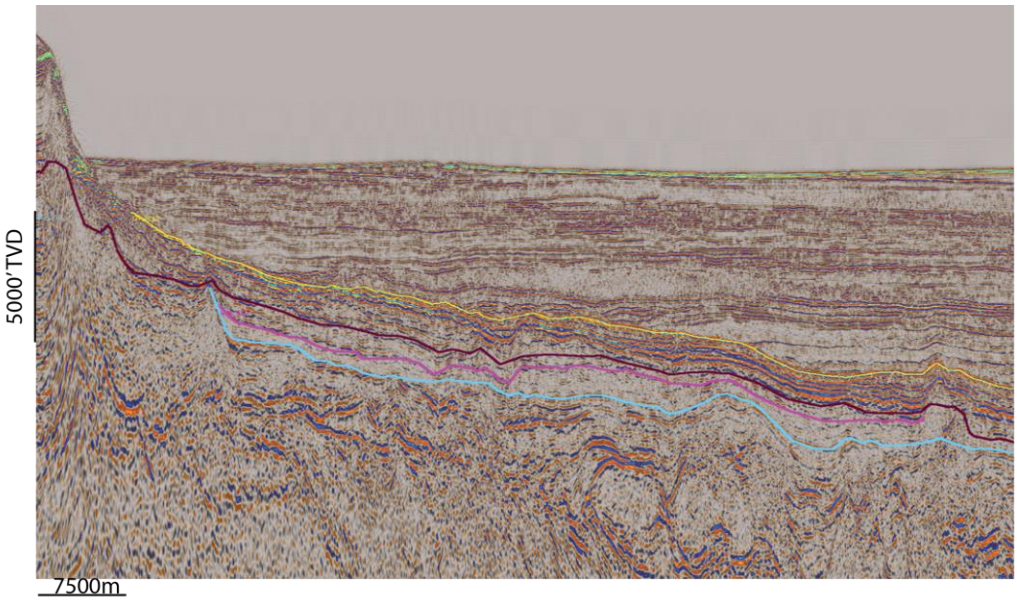

Figure 30: 2D seismic strike view of the Hosston progradational sandy delta-fed apron where incision becomes evident. Top Navarro-Taylor (yellow), Top Sligo (maroon), Top Hosston (pink), Top Cotton Valley Knowles (blue).Seismic data courtesy Fugro.

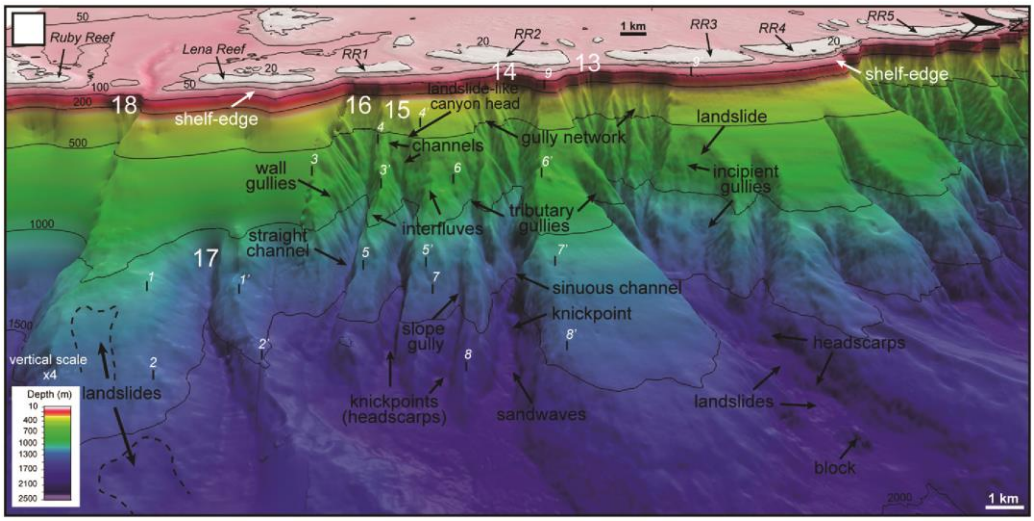

Figure 31: DEM cross-section view of shelf-incised canyons and adjacent reef-blocked areas in the Ribbon Reef region of the Great Barrier Reef, Australia showing canyon morphology and related morphological features. The Valanginian-Hauterivian-aged Florida Escarpment could have contained the same features adjacent to the progradational sandy delta-fed apron. (Modified from Puga-Bernabéu et al., 2011).

PROGRADATIONAL SANDY DELTA-FED APRON

An apron is used to describe various deposits on the shelf, slope, and basin (Galloway, 2002). In contrast to well-organized, point-sourced submarine fans, slope aprons form as a linear depositional "belt" that is lateral to submarine fans and is dominated by hemipelagic mud sedimentation or mass transport processes rather than a predominance of sandy turbidity flows in well-defined channels and lobes (Gorsline and Emery, 1959; Reading and Richards, 1994). It is common that slumps and slope failures bring carbonate rim material down the slope and deposit at the base of the slope in a toe-of-the-slope apron, extending parallel to the shelf edge (Playton et al., 2010). Stow (1981) proposed that under lower sea level conditions, when the coastal system was more proximal to the shelf edge, sands may have been deposited on slope aprons by turbidity currents (Reading and Richards, 1994).

Our definition of an apron is a sandy deposit at the toe-of-the-slope, extending linearly, parallel to the shelf edge, lateral to submarine fans, and fed by siliciclastic material derived from line sourced systems including deltas and shore zones (Galloway, 2002). Line sources could also a series of include small scale-entry points where the shelf margin reef is breached. The latter part of this definition is consistent with that of Reading and Richards (1994) of sand-rich linear-source slope aprons: collapse of shelf clastics (e.g. during storms) generates low-efficiency turbidity currents, supplying the apron; a channel system of poorly developed transitory channels and multiple chutes; lower fan sediments of fleeting sandy turbidity flows (Figure 32). To distinguish the GBDS sandy apron from carbonate grain aprons, it is termed the sandy progradational delta-fed apron deposystem (Galloway, 2002). Ocean currents can potentially play a role in the depositional body geometry, helping to enhance the apron structure at the toe of the slope (Snedden et al., 2012).

The type of sand-rich apron proposed for the Valanginian-Hauterivian in the eastern Gulf of Mexico is relatively unknown because not many modern examples exist. Wezel et al. (1981) describe the sand-rich apron found along the tectonically active Sardinia-Tyrrhenian margin and suggest currents sweep the shelf and carry sands out of closely spaced channels (Reading and Richards, 1994). Reading and Richards (1994) suggest two additional processes by which the apron sands are derived: sands brought to coastal braid plains by a drop in relative sea level (such as in southeast Asia or New Zealand, where continents and islands are actively uplifted); during a relative sea level low when the coastal plain was proximal to the shelf edge (such as has occurred in Nova Scotia).

Reading and Richards (1994) also cite Kumar and Slatt's (1984) work on the Pennsylvanian-age Tonkawa sandstone of Oklahoma, in which they document 200-km-long sands deposited on a slope apron. Without well control over the body of the apron, we

rely on seismic data and a limited number of modern analog systems to guide our interpretation.

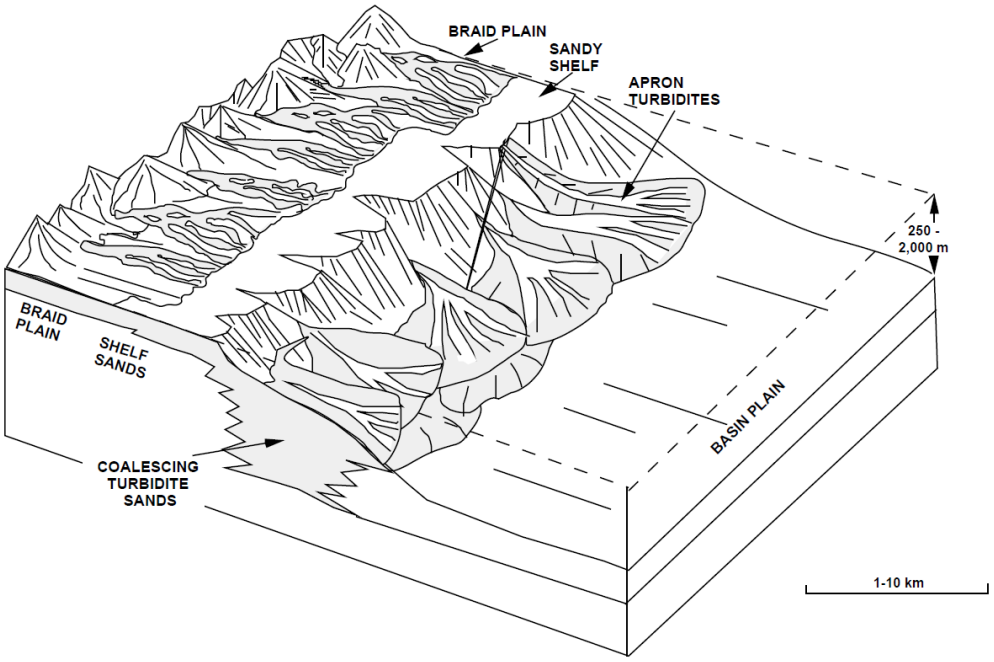

Figure 32: Schematic diagram of a linear-source sand-rich slope apron and related depositional environments (Reading and Richards, 1994).

MISSISSIPPI CANYON ASYMMETRIC EXPULSION ROLLOVERS

The hypothesis for the Valanginian-Hauterivian time in the eastern Gulf, including Mississippi Canyon, was that sediment was delivered to the deep-water in a NE-SW trending direction, potentially feeding the salt-generated asymmetric expulsion rollovers observed in Mississippi Canyon. These salt evacuation features, which can look like a 3000 m-scale clinoform to the untrained eye, preserve progradational and sediment transport direction, unlike turtle structures (Ge et al., 1997).

Interpretation of 3D seismic data reveals a two-phase growth history of the asymmetric expulsion rollovers. The first is from Cotton Valley-Bossier Tithonian time to

Cotton Valley-Knowles Berriasian time, in which the Cotton Valley-Knowles supersequence was deposited in a thick carbonate succession, resulting in continuous, strong reflections in seismic (Figure 19). The Cotton Valley-Knowles in overlain by the Hosston, which is a relatively thin package in the deep-water. The Hosston to the Sligo time interval was another growth phase in the rollover. With the 590 ft (180 m) of the Sligo formation preserved in the MC 392 #1 Appomattox well above the Hosston, plus 2395 ft (730 m) of Navarro-Taylor through Bexar-Pine Island deposition, the asymmetric expulsion rollover section found west of the MC 392 #1 Appomattox well is interpreted to be largely Late Cretaceous in age. The uniform thickness of the deposits between Sligo time and Navarro-Taylor time suggests a period of salt tectonic quiescence, supporting McDonnell's work (2010).

The numerous salt evacuation features disrupt seismic interpretation of the Hosston in many of the asymmetric expulsion rollovers of Mississippi Canyon, which lose reflectivity and continuity in the transition to a new rollover. Yet the bright reflections of the Navarro-Taylor supersequence at the top of the Cretaceous are more easily distinguished and it can be inferred that the Hosston section comprises some part of the asymmetric expulsion rollovers throughout Mississippi Canyon. However, the exact thickness and extent of the Hosston in additional asymmetric expulsion rollovers remains guesswork until new drilling penetrates these large structures.

SEISMIC FACIES MAPPING

With evidence of such medium-grained sandstone cored in the Stanolind-Sun Perpetual Forest #1 well (onshore Florida), and linkage with such a proximal sediment source, the potential for high porosity and permeability reservoir rocks in the Valanginian-Hauterivian sandy progradational delta-fed apron is considerable. Seismic facies mapping

of the Valanginian-Hauterivian dim seismic facies (interpreted to be sand) suggests the apron is roughly parallel to the modern Florida shelf edge and extends for 200 km.

Mapping of the Hosston section in the Mississippi Canyon deep-water area reveals that the dim sand facies extends in wedges only approximately 70 km off the shelf edge. The limited extent of deposition suggests low sediment supply, indicating only a small part of the southern Appalachians served as the source terrane for the Mississippi Canyon Hosston deposits, which is consistent with the source-to-sink scaling relationships studied for the Appalachian-sourced system, although smaller than the relationships predict (see Fan Runout Length Prediction on page 56).

Published global charts, built on seismic records and biostratigraphy, indicate that eustatic sea level was high and generally rising in the Valanginian-Hauterivian time (Snedden and Liu, 2011). With the deposition of the Valanginian-Hauterivian Hosston formation, several sequence stratigraphic surfaces and systems tracts are interpreted in a North-South onshore-to-deep-water stratigraphic dip cross section (Figure 20). Most of the proximal systems tracts identified are transgressive and highstand systems tracts, as interpreted from gamma ray and resistivity log character (Mitchum et al., 1994). Using seismic interpretation as a guide, along with the prominent resistivity decrease through the Hosston interval of DC 353 #1 Vicksburg B well – interpreted to be a silty package of low-density turbidites – one can interpret the distal portion of a lowstand systems tract slope system.

SOURCE-TO-SINK

Two distinct age populations found in the Stanolind-Sun Perpetual Forest #1 well upper sample (4180-4700ft MD), 493-699 Ma and 1992-2240 Ma, correspond with the Brasiliano/Pan-African orogeny and Trans-Amazonian/Eburnean Craton respectively

(Suwannee terrane; Figure 25; Dallmeyer, 1989; Park et al., 2010). Notably suppressed in the zircon age populations is the 950-1300 Ma range that corresponds with the Grenville orogeny associated with the Appalachian foreland basin (Park et al., 2010). This absence of a Grenville 950-1300 Ma peak for the upper sample (4180-4700ft MD) suggests the younger Hosston siliciclastics of the Stanolind-Sun Perpetual Forest #1 well were not sourced by the Appalachian Mountains.

Age populations found in the the Stanolind-Sun Perpetual Forest #1 well lower sample (4700–5230ft MD), 514-699 Ma and 2050-2168 Ma, correspond with the Brasiliano/Pan-African orogeny and Trans-Amazonian/Eburnean Craton respectively (Figure 26; Dallmeyer, 1989; Park et al., 2010). Like the upper sample of the Stanolind-Sun Perpetual Forest #1 well, the lower portion of the well (4700–5230ft MD) does not contain an age population that corresponds with the Grenville orogeny, suggesting a source terrane other than the Appalachian Mountains (Park et al., 2010).

The presence of the Suwannee zircons in the Stanolind-Sun Perpetual Forest #1 well at the Valanginian-Hauterivian stages suggests a peninsular Florida source terrane for the Valanginian-Hauterivian Hosston siliciclastics in the progradational sandy delta-fed apron observed in the eastern GOM. The Suwannee terrane, comprised of Gondwanan/Peri-Gondwanan material, was sutured to the North American craton 300 Ma during the Alleghanian Orogeny with tholeiitic basalts and diabases, as well as felsic and intermediate volcanic rocks comprising the Suwannee basement (Heatherington and Mueller, 2003; Dallmeyer, 1989). The Suwannee terrane's U-Pb detrital zircon geochronologic signature is that of the Gondwanan crust, coeval with the Brasiliano/Pan-African (530-680 Ma) and the Trans-Amazonian/Eburnean (2000-2200 Ma) cratons (Becker at al., 2005, 2006; Park et al., 2010). The U-Pb age populations of the Hosston

interval of Perpetual Forest #1 are similar to that of the Paleozoic basement interval sampled by Lisi (2012) in Florida state waters (Figure 33).

We believe the Suwannee basin was then uplifted coincident with termination of GOM sea-floor spreading, at approximately 137 Ma, forming the Ocala Arch. The Ocala Arch, primed for erosion, then served as the source terrane for the Valanginian-Hauterivian siliciclastics found in the Stanolind Sun Perpetual Forest #1 well, and arguably the down-dip Valanginian-Hauterivian siliciclastics in the progradational delta-fed apron as well. With no known well penetrations of Valanginian-Hauterivian deep-water sandstones as of this writing, additional detrital zircon analysis cannot be included in this study.

However, we can infer possible deep-water transport from the orientation of the asymmetric expulsion rollovers found in the Mississippi Canyon deep-water which we believe preserve the progradation direction of original sedimentation. As seen in Figure 9, the asymmetric expulsion rollover prograded from ENE to WSW, indicating a possible connection to the southern Appalachian source terrane. To better verify the source terrane of the Valanginian-Hauterivian siliciclastics, additional U-Pb detrital zircon analysis should be done in onshore, shelf, and deep-water core samples when these become available. Still, the age populations and indication of the Suwannee basin found in the Stanolind-Sun Perpetual Forest #1 sample are compelling contributions to the understanding of the evolution of the eastern GOM basin.

APPALACHIAN-SOURCED FAN RUNOUT LENGTH PREDICTION

The modern Chattahoochee River is 692 km long and feeds into the Apalachicola River, which itself is 170 km in length (Couch et al., 1996). Based on seismic mapping and interpretation, it is feasible that the DeSoto Canyon and Mississippi Canyon Appalachian-sourced fan was fed by the paleo-Chattahoochee-Apalachicola River system. Thus, when

considering the river length upon which fan length predictions are made in the Somme et al. (2009) empirical relationships, it is reasonable to use a river length from the Chattahoochee-Apalachicola River system. A length of 887 km is significantly shorter than the same pathway drawn following the exact path of the modern Chattahoochee-Apalachicola fluvial system (1107 km; Table 2). The predicted fans of these two river channel lengths are both significantly shorter than that predicted from the river channel length extending to the Blum and Pecha (2014) drainage divide (Figure 15).

Seismic facies mapping of the dim (low amplitude), sandy seismic facies indicates the interpreted fan length of the Mississippi Canyon fan is about 70 km. This is shorter than what is expected from any of the three river paths based on the Somme et al. (2009) river length-fan length relationship (Table 2). Somme et al.'s (2009) scaling relationships are primarily defined in modern and Quaternary source-to-sink systems which lack the influence of salt tectonics. The great accommodation space created by the salt-influenced asymmetric expulsion rollovers most likely limited progradation of Valanginian-Hauterivian sediments in Mississippi Canyon, resulting in a shorter fan length than Somme et al.'s (2009) model predicts. By analogy, Paleogene Upper Wilcox sands did not prograde into the deep-water but terminated in onshore Texas due to the tremendous accommodation space generated by onshore Texas growth faults (Fiduk et al., 2004; Galloway, 2008; Galloway, pers. comm.). Similarly, the generous accommodation space created by the asymmetric expulsion rollovers in Mississippi Canyon probably hindered the continued progradation of Valanginian-Hauterivian sands and resulted in a fan shorter than predicted by the Somme et al. (2009) method.

A fan length of approximately 90 km, which could be produced by a paleo-Chattahoochee-Apalachicola river system with headwaters in the same location as the present-day Chattahoochee River, extends far beyond the reach of the dim (low amplitude)

seismic facies observed in the 2D and NAZ 3D data (Figure 34). However, the length of the fan could be extended by accounting for the distance the 45 m-thick Hosston sands encountered in the MC 379 #1 well were displaced due to salt rafting. By using an average distance of rafting of the Norphlet formation in the late Jurassic time calculated by others (46 km; Snedden, pers. comm.; Hudec, pers. comm.; Fiduk et al., 2014), we can apply that distance to the overturned block found in MC 379 #1, bringing the Hosston sands back to a location northeast of the MC 379 #1 well that restores a change in fan length of 90 km (Figure 34). This location is remarkably similar to the edge of the fan originally interpreted to correspond with the paleo-Chattahoochee-Apalachicola river system (Figure 34), and makes a case for a possible larger fan geometry and best-case scenario.

The river channel that extends to the Blum and Pecha (2014) drainage divide (Figure 15), which yields a fan length of 135-674 km, is nearly twice as long as seismic facies mapping indicates the fan extends. This interpretation is considered least likely. Based on seismic facies observation and the assumption that incision has extended the length of the Chattahoochee River since the Valanginian-Hauterivian time, a fan length of approximately 70 km and river length of 700 km is considered the most likely fan geometry and the preferred interpretation here. This shorter axial length of the sandy fan implies many of the ENE-WSW-oriented asymmetric expulsion rollovers in Mississippi Canyon may be sandstone-poor or deficient.

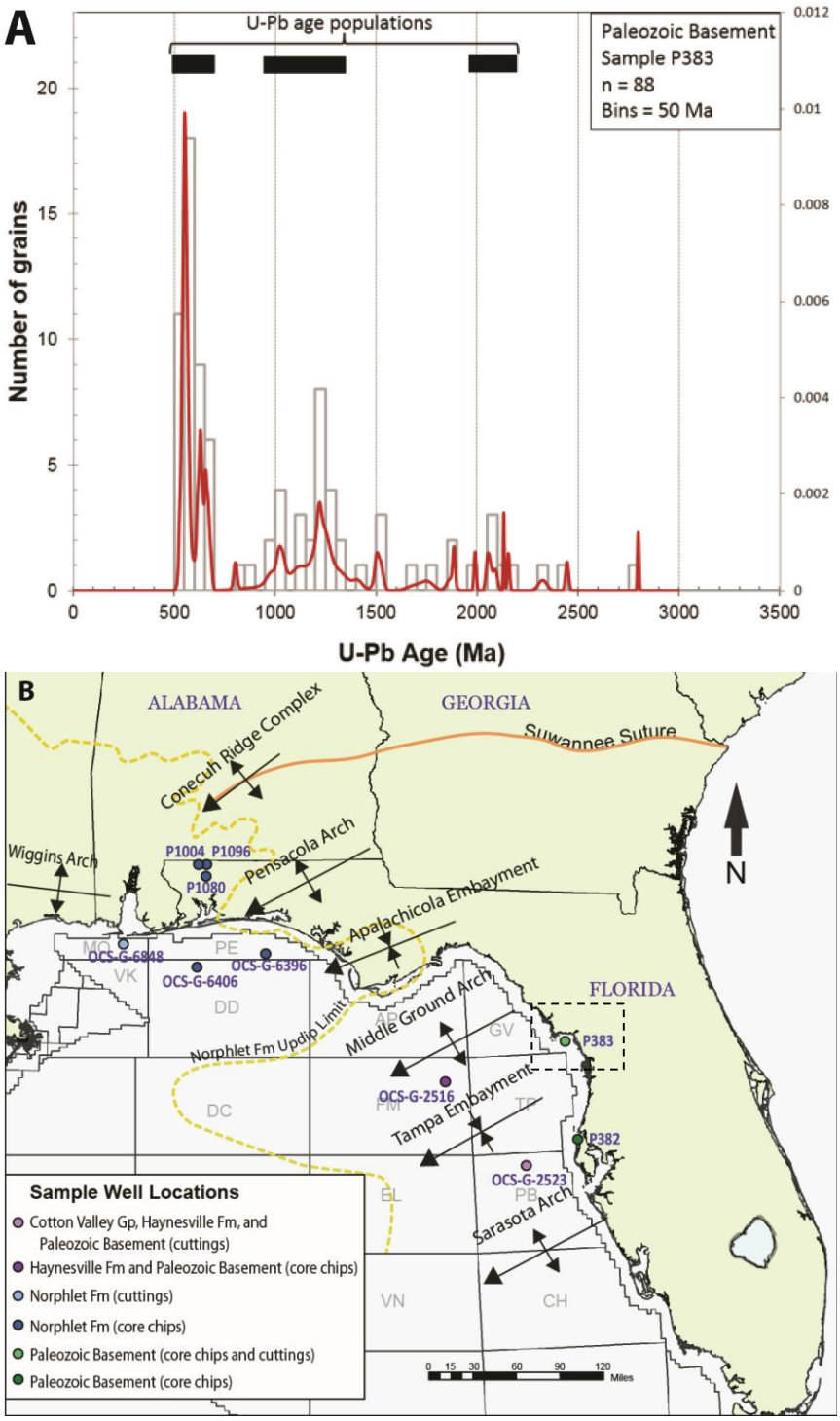

Figure 33: A) U-Pb age populations sample from Paleozoic basement interval of Florida state waters; B) Location of Paleozoic basement sample. (Modified from Lisi, 2012).

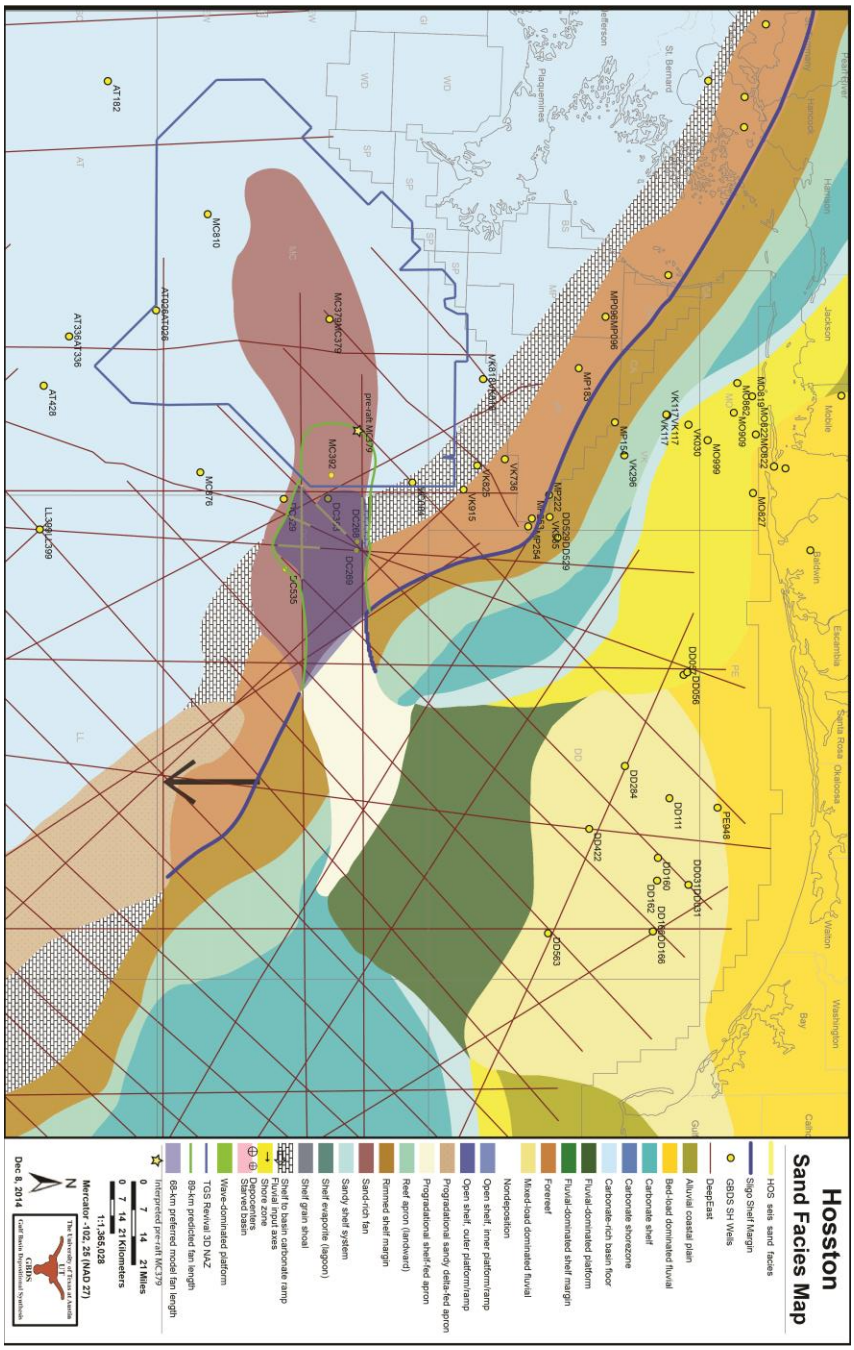

Figure 34: 70-km fan (blue; preferred model) drawn based on seismic facies mapping (yellow) compared with a 90-km fan (green) and hypothesized fan (maroon). Interpreted pre-raft location of MC379 sands (star). The 90-km fan extent reaches beyond where the fan is observed in seismic and corresponds to paleo-Chattahoochee River headwaters located in the same position as the present day.

Chapter 5: Conclusions

This study provides an assessment of two source-to-sink systems of the early Cretaceous and highlights the sedimentological changes that occurred in response to major tectonic reorganization of the eastern Gulf of Mexico. A seismically-defined boundary exists between the siliciclastic Valanginian-Hauterivian Hosston and overlying carbonate Barremian Sligo formations in the eastern Gulf of Mexico shelf and deep-water, where it was previously thought to be a gradational contact. U-Pb dating of detrital zircon grains tells us the Valanginian-Hauterivian Hosston siliciclastics observed in the 200-km-long base-of-slope sandy progradational delta-fed apron at the Florida Escarpment originate in a peninsular Florida source terrane – the Ocala Arch. Without the inclusion of U-Pb detrital zircon analysis in this study, researchers might have continued to assume the Valanginian-Hauterivian Hosston of the entire eastern Gulf of Mexico was sourced by the Appalachian Mountains, and overlooked the possibility of a sandstone reservoir in the eastern Gulf with favorable reservoir quality and volume. Interpretation of 3D seismic data with nearby well-control allows conclusions to be drawn about the Appalachian-sourced Valanginian-Hauterivian Hosston fan system in Mississippi Canyon. This Appalachian-sourced sandy fan is believed to have terminated updip of the asymmetric expulsion rollovers, although we know the asymmetric expulsion rollover deposition was coeval to the Valanginian-Hauterivian Hosston, and extended from the Cotton Valley-Bossier supersequence to the Navarro-Taylor supersequence time. The sand-rich fan is interpreted to have been deposited in a lowstand systems tract, which is also observed in the onshore western Gulf of Mexico Travis Peak formation (Ewing, 2010). Two plausible models of Appalachian-sourced fan length are considered, incorporating recent calculations of salt rafting to estimate a best-case scenario fan length of 90 km, while a more certain fan geometry is

determined from seismic observations and well control, yielding a Valanginian-Hauterivian fan of 70-km-length. The study presents a new model of Hosston paleogeography, with special focus on the eastern Gulf of Mexico and the sand-rich fan and sandy progradational delta-fed apron and its delta pathway. It also provides a rich and robust model for source to sink transport during a critical phase of Gulf of Mexico evolution. The implications for exploration are significant. The shorter fan length calculated in this study suggest the majority of asymmetric expulsion rollovers in Mississippi Canyon are either sandstone-poor or were sourced from a different, likely younger, source-to-sink system (e.g. Late Cretaceous Cenomanian-aged).

Appendices

APPENDIX A

We originally sampled the Magnolia State 5B #1 well, drilled in Florida state waters near the Apalachicola protraction block, , but subsequent to sampling, determined this interval to be younger than Valanginian-Hauterivian time.

The Florida Geological Survey in Tallahassee maintains core chips and cuttings from the Magnolia State 5B #1 well. Samples from each 10-foot interval were examined and the average grain size for each sample was obtained. From these observations, a grain size distribution was calculated in Excel and a weathering profile log drawn in Adobe Illustrator. Grain size of the sampled interval, now believed to be the Paluxy-Washita formations, in the Magnolia State #5B well ranges from fine to coarse sand grains. 44% of the observed samples were found to be medium grained. 20% of the observed samples were found to be coarse-grained, and 20% fine-grained.

The medium-grained sands found in the Magnolia State #5B well indicate the Paluxy-Washita sands are in relative close proximity to their source, however, the increased proportion of fine-grained sands relative to the Stanolind-Sun Perpetual Forest #1 well suggest a longer transport length. The micaceous sands of the Magnolia State #5B well visually appear to be of a different source terrane than the sands of the Stanolind-Sun Perpetual Forest #1 well. Still, the similar grain size distributions of the sands of the two wells suggests the source terrane for the Magnolia State #5B sands might be limited to a smaller portion of the Appalachians, not the entire Grenville province.

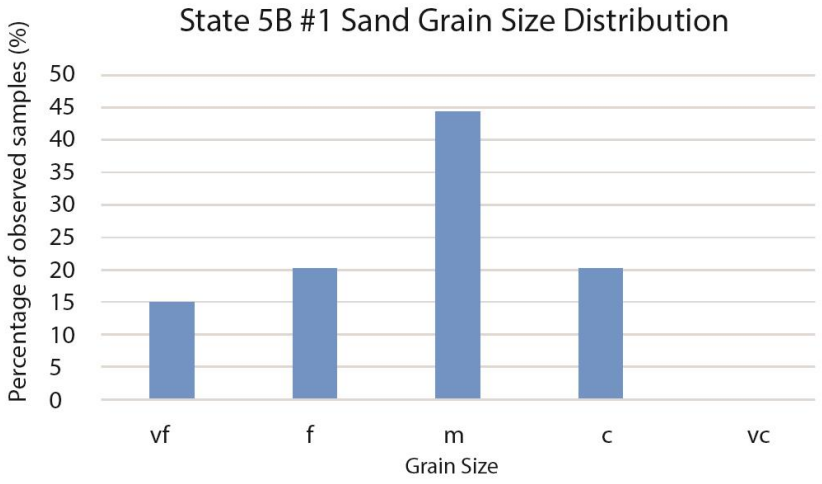
State 5B #1 Sand Grain Size Distribution
Percentage of observed samples (%)
50
45
40
35
30
25
20
15
10
5
0
vf
f
m
c
vc
Grain Size

Magnolia State #5-B, Franklin County, Florida
Core Chip Description

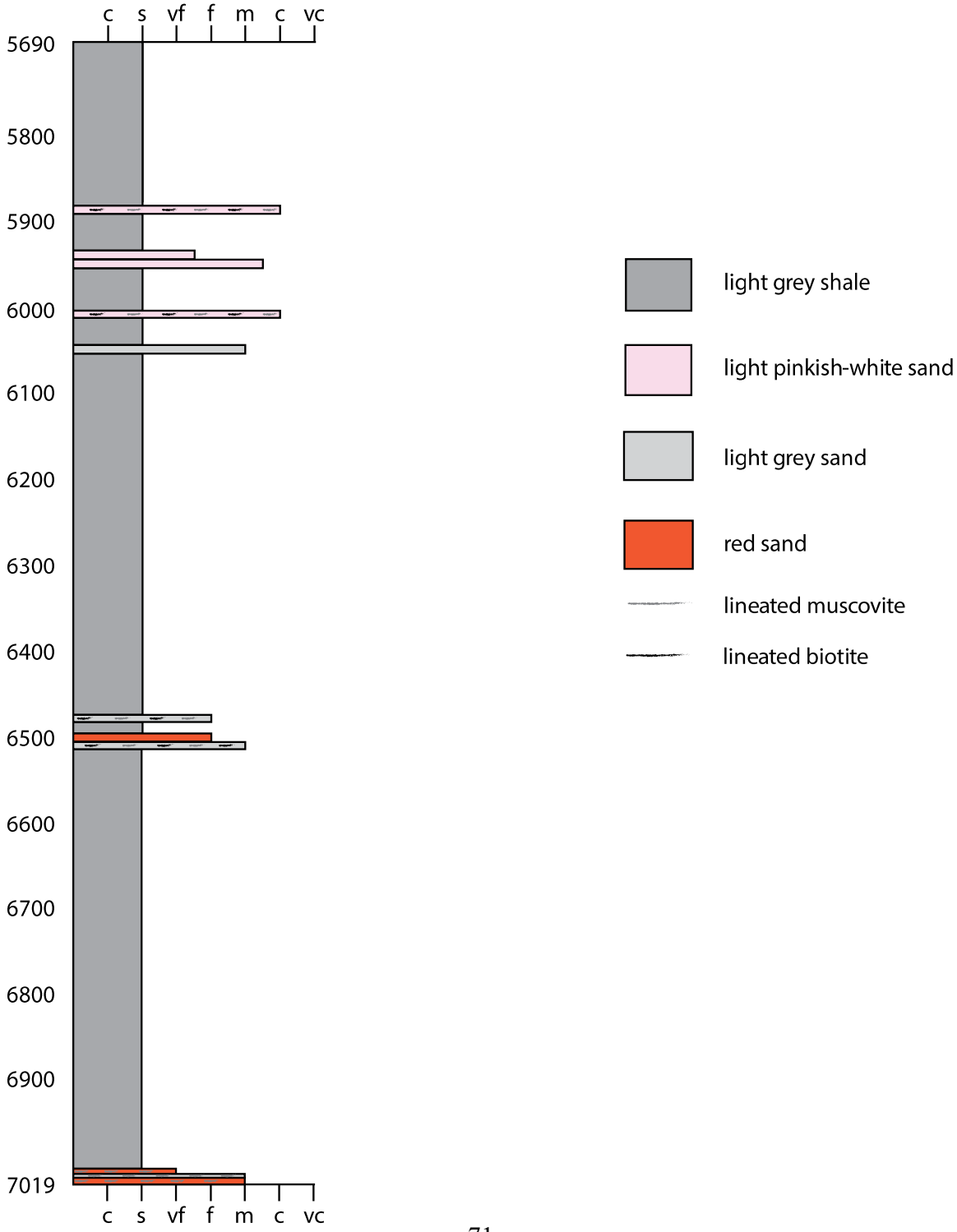

Magnolia State #5-B, Franklin County, Florida
Core #23 Chip Description

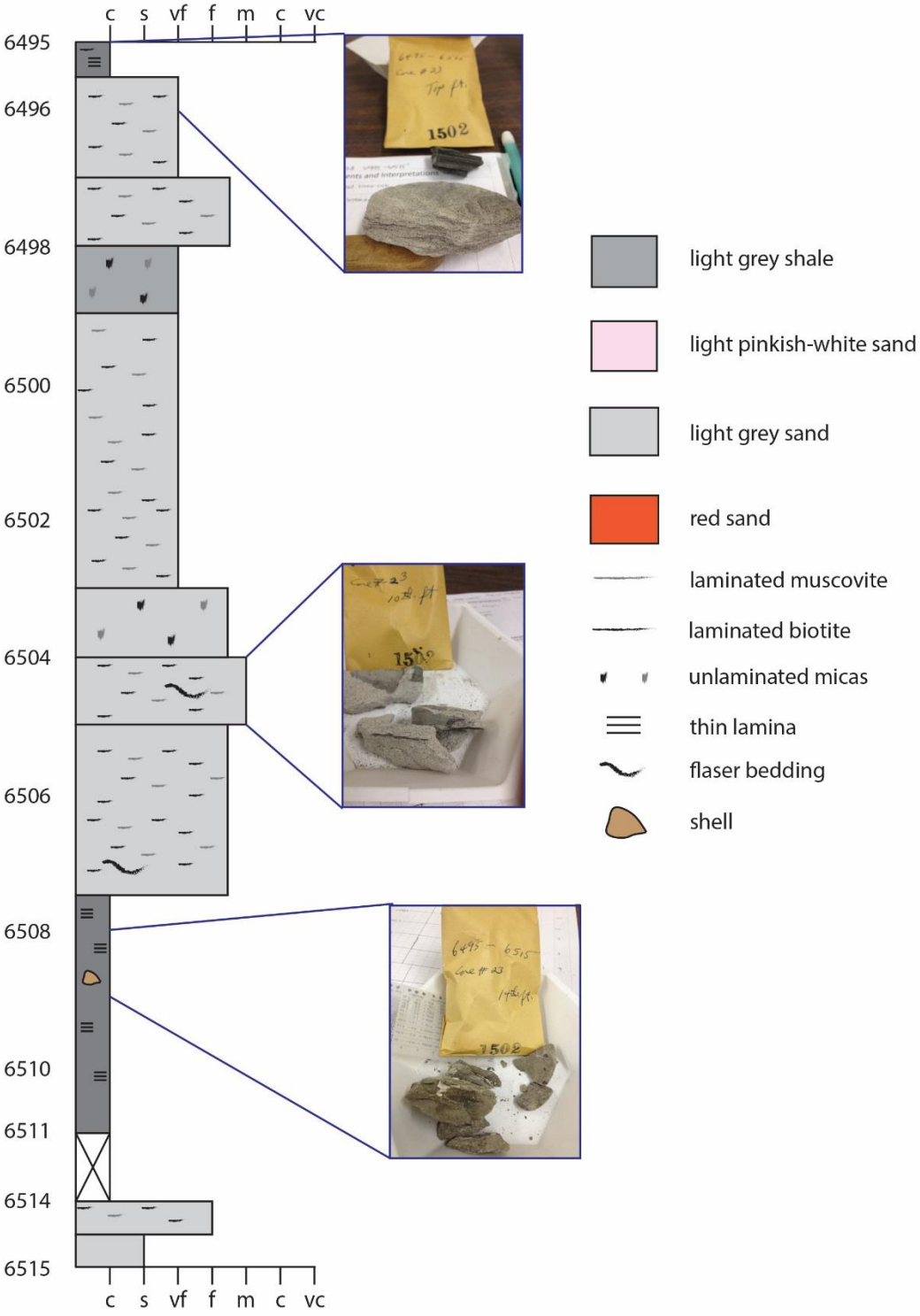

Magnolia State #5-B, Franklin County, Florida
Core #24 Chip Description

APPENDIX B

U-Pb Data Table, Stanolind-Sun Perpetual Forest #1 Upper Half (4180-4700ft MD)

PFUpper					207/235		206/238		207/206		
Grain #	[U] ppm	U/Th	207/235	206/238	Age Ma	2σ error	Age (Ma)	2σ error	Age (Ma)	2σ error	% Disc
57	483	1.10	0.33780	0.04692	295.3	4.1	295.5	3.6	289	40	0.1
98	872	0.97	0.37830	0.04852	325.7	3.2	305.4	3.4	456	31	6.2
18	692	0.87	0.36570	0.05003	316.3	4.0	314.7	3.7	326	31	0.5
51	99.5	0.88	0.36500	0.05234	315.3	8.7	328.8	6.0	218	73	4.3
2	352	1.46	0.48700	0.06350	402.4	7.4	398.0	8.2	420	52	1.1
66	510	1.55	0.63310	0.07950	497.9	5.2	493.3	6.5	515	31	0.9
77	131	1.25	0.64000	0.07970	503.2	9.2	494.2	6.7	534	48	1.8
84	82.4	1.04	0.67600	0.08100	525.0	15.0	502.3	9.0	589	89	4.3
29	257.6	0.77	0.65800	0.08207	513.0	7.3	508.4	5.8	544	40	0.9
97	231.3	0.97	0.65800	0.08210	514.6	7.3	508.4	6.0	574	42	1.2
96	95.7	1.38	0.65600	0.08320	513.0	11.0	515.4	6.8	491	60	0.5
10	234.8	0.78	0.67900	0.08370	525.9	7.0	518.3	6.0	550	37	1.4
73	272	3.07	0.66700	0.08380	518.8	6.2	519.0	6.2	511	33	0.0
95	83.4	1.19	0.68200	0.08530	532.0	12.0	527.9	6.9	537	58	0.8
43	129	1.01	0.70500	0.08560	541.9	9.3	529.2	5.9	559	46	2.3
4	151	1.29	0.69300	0.08570	535.0	7.6	531.2	7.3	558	42	0.7
20	176.1	1.83	0.68800	0.08602	531.1	6.3	531.9	5.5	535	37	0.2
109	515	2.30	0.71090	0.08600	545.0	5.6	532.1	6.0	590	33	2.4
88	175.5	1.86	0.69800	0.08700	537.0	13.0	538.0	11.0	583	79	0.2
50	131	1.22	0.71400	0.08720	547.3	9.9	539.0	11.0	579	53	1.5
58	493.5	2.00	0.70200	0.08720	539.8	8.3	539.0	16.0	598	50	0.1
3	156.7	0.99	0.71300	0.08740	546.2	8.2	539.9	7.2	588	47	1.2
22	98.9	0.87	0.75700	0.08740	570.0	18.0	539.9	9.1	700	86	5.3
64	59	2.38	0.70500	0.08760	540.0	13.0	541.0	9.2	529	74	0.2
71	124.1	0.98	0.72000	0.08770	550.1	8.7	541.9	7.8	556	51	1.5
82	515	17.72	0.71500	0.08780	547.4	7.5	542.8	7.5	599	47	0.8
116	139	1.02	0.72100	0.08830	550.5	8.1	545.6	9.6	555	52	0.9
107	70.2	0.83	0.72300	0.08850	551.0	12.0	546.6	9.6	591	60	0.8
94	177	0.91	0.73000	0.08870	556.0	7.5	547.8	6.9	553	39	1.5
99	221	1.53	0.72100	0.08870	551.8	8.1	547.8	6.3	543	41	0.7
92	81.7	0.80	0.73100	0.08910	556.0	11.0	550.2	7.9	580	52	1.0
117	314	1.14	0.72560	0.08921	553.6	5.8	550.8	5.1	545	31	0.5
48	140.7	0.43	0.71700	0.08930	550.0	8.5	551.5	6.9	532	50	0.3

89	268.5	0.95	0.73200	0.09000	557.7	8.1	555.2	8.3	580	42	0.4
110	92.9	1.80	0.70900	0.09010	544.3	9.5	556.2	8.1	504	46	2.2
21	152	0.75	0.74100	0.09030	562.8	6.9	557.2	6.3	600	40	1.0
104	181	1.65	0.73500	0.09054	558.9	7.3	558.7	5.1	560	35	0.0
26	323.2	32.40	0.74400	0.09060	563.0	13.0	558.8	7.7	618	39	0.7
11	73.9	0.85	0.77300	0.09200	580.0	12.0	567.3	7.6	605	60	2.2
5	248	1.54	0.76400	0.09250	576.1	6.2	570.1	6.2	578	31	1.0
25	299	4.70	0.76200	0.09260	574.9	7.9	570.9	9.1	630	45	0.7
74	103	0.86	0.76700	0.09290	577.0	10.0	574.8	8.5	592	52	0.4
59	129	2.08	0.80100	0.09340	595.0	19.0	575.0	17.0	677	56	3.4
41	637	1.92	0.77800	0.09320	584.0	6.3	575.2	7.7	603	26	1.5
87	123.1	13.20	0.75900	0.09340	572.7	9.6	575.3	7.3	556	46	0.5
52	78.6	0.87	0.77600	0.09400	583.2	9.5	580.3	8.6	603	50	0.5
123	31	0.43	0.84600	0.09440	622.0	19.0	581.0	12.0	773	89	6.6
70	65.1	1.50	0.77000	0.09440	578.0	12.0	581.5	8.0	539	58	0.6
55	159	1.32	0.76700	0.09472	577.5	8.3	583.4	5.8	569	35	1.0
102	178.3	0.57	0.79400	0.09500	592.7	7.6	584.8	6.4	594	41	1.3
16	142	1.06	0.81500	0.09640	607.0	14.0	593.0	11.0	664	84	2.3
105	138.8	3.27	0.83000	0.09650	614.0	10.0	593.9	8.4	686	46	3.3
27	35.9	0.96	0.82300	0.09690	606.0	24.0	596.0	14.0	670	93	1.7
19	63.8	1.59	0.82300	0.09710	612.0	14.0	597.0	11.0	720	66	2.5
23	108	0.68	0.80100	0.09710	597.5	9.2	597.4	8.3	624	53	0.0
36	47.9	0.65	0.80300	0.09720	600.0	12.0	598.0	10.0	564	68	0.3
115	149	0.95	0.81800	0.09720	611.0	14.0	598.0	11.0	599	41	2.1
80	176.2	1.00	0.81000	0.09740	602.2	5.8	598.8	6.1	618	33	0.6
119	128.4	0.97	0.81800	0.09750	606.2	8.4	599.6	7.3	620	41	1.1
63	262	0.51	0.81610	0.09800	606.3	5.4	602.9	6.5	619	27	0.6
118	174.7	2.87	0.81500	0.09810	606.4	7.3	603.0	6.1	600	38	0.6
17	232.3	1.41	0.82200	0.09810	609.9	7.7	603.4	7.5	627	45	1.1
86	697	5.94	0.81900	0.09850	607.0	11.0	606.0	14.0	633	43	0.2
46	75.9	1.35	0.83400	0.09860	614.0	11.0	606.3	8.1	624	60	1.3
68	309	6.27	0.82720	0.09866	611.8	5.3	606.5	5.4	610	27	0.9
85	36.9	1.15	0.83800	0.09870	618.0	18.0	607.0	13.0	650	100	1.8
34	258	1.95	0.83500	0.09894	616.0	7.5	608.8	5.6	629	33	1.2
6	311	0.98	0.84800	0.09940	623.1	7.3	611.1	6.0	651	31	1.9
44	279	0.79	0.82600	0.09950	612.5	7.0	611.7	7.1	596	28	0.1
40	364.3	2.06	0.85000	0.09957	624.9	6.0	611.8	5.6	652	28	2.1
122	80.1	0.83	0.83000	0.10010	613.0	12.0	615.0	12.0	627	48	0.3

100	304	1.69	0.83800	0.10080	618.6	7.0	619.1	8.0	607	36	0.1
56	33.8	1.37	0.83500	0.10110	617.0	15.0	620.0	14.0	627	81	0.5
83	44.1	1.13	0.87300	0.10140	638.0	16.0	622.0	12.0	708	73	2.5
31	128	1.23	0.86300	0.10140	632.6	9.1	622.3	7.4	679	45	1.6
61	116	0.87	0.87000	0.10180	635.0	10.0	624.9	8.1	696	51	1.6
37	224.5	2.27	0.87600	0.10250	640.2	6.8	629.3	6.1	643	29	1.7
49	152.8	2.87	0.84100	0.10290	621.0	11.0	631.4	9.4	604	56	1.7
65	149.3	1.39	0.92200	0.10760	662.8	8.9	659.0	11.0	703	46	0.6
12	394	2.10	0.94300	0.10930	674.0	7.7	668.5	5.8	664	26	0.8
120	98	0.55	0.93700	0.11090	671.0	12.0	678.1	9.3	640	47	1.1
42	174.8	2.66	1.01100	0.11220	712.0	13.0	685.0	13.0	759	45	3.8
1	69.7	1.85	1.01200	0.11430	711.0	17.0	699.0	14.0	736	58	1.7
81	295	4.67	1.13100	0.12620	767.7	8.8	766.3	8.4	797	35	0.2
75	183	3.05	1.29500	0.13950	843.0	26.0	841.0	28.0	833	34	0.2
15	87.3	0.83	1.59300	0.15520	967.0	14.0	930.0	17.0	1018	48	3.8
69	52.5	2.34	1.74800	0.17250	1026.0	15.0	1026.0	14.0	1039	48	1.3
13	116	2.14	1.82600	0.17330	1054.0	20.0	1030.0	16.0	1088	35	5.3
112	371.2	5.19	1.90100	0.18170	1080.7	7.8	1076.0	11.0	1094	19	1.6
113	84.7	0.80	1.87000	0.17890	1070.0	10.0	1061.0	13.0	1102	32	3.7
106	39.8	1.19	2.50100	0.22040	1274.0	14.0	1284.0	18.0	1260	40	1.9
32	182.5	2.86	2.73800	0.22820	1338.0	14.0	1325.0	14.0	1323	39	0.2
72	241.5	0.84	2.65400	0.22210	1315.1	7.7	1292.9	8.3	1344	13	3.8
101	256.8	1.74	2.60700	0.22280	1302.0	11.0	1296.0	17.0	1347	24	3.8
24	103.3	1.00	4.45400	0.30700	1721.0	11.0	1728.0	14.0	1748	21	1.1
60	83.3	1.01	4.96300	0.31720	1813.0	11.0	1775.0	18.0	1864	22	4.8
93	293	1.95	5.58000	0.33080	1912.0	16.0	1842.0	26.0	1952	15	5.6
35	434.7	4.65	6.20700	0.36020	2005.1	8.0	1983.0	18.0	1992	15	0.5
124	162.4	0.93	5.00000	0.28990	1818.0	18.0	1640.0	29.0	2011	24	18.4
78	91.3	1.35	6.52900	0.37390	2049.4	8.1	2047.0	21.0	2052	21	0.2
7	410	4.11	6.00600	0.34380	1977.7	8.4	1905.0	20.0	2056	16	7.3
67	44.1	1.28	6.25800	0.35220	2011.0	13.0	1944.0	22.0	2064	25	5.8
90	199	1.23	6.61700	0.37390	2062.0	7.9	2047.0	15.0	2068	14	1.0
9	14.26	6.56	6.29000	0.35400	2020.0	43.0	1965.0	52.0	2070	81	5.1
108	79.6	1.38	7.16000	0.40520	2134.0	12.0	2192.0	26.0	2072	26	5.8
14	191.7	0.67	6.67600	0.37160	2069.1	8.3	2037.0	19.0	2092	18	2.6
79	293	13.00	6.82400	0.38010	2089.2	8.2	2076.0	15.0	2102	10	1.2
103	34.11	2.52	6.10700	0.33680	1993.0	11.0	1870.0	23.0	2103	25	11.1
28	202	1.38	6.59000	0.36560	2056.0	18.0	2008.0	33.0	2117	20	5.1

30	247.3	1.98	6.60400	0.36800	2059.0	11.0	2020.0	18.0	2120	17	4.7
47	153.6	1.53	7.18700	0.38840	2134.3	7.8	2115.0	17.0	2154	14	1.8
39	274	1.42	7.32600	0.39080	2151.6	6.6	2126.0	11.0	2171	9	2.1
38	78	1.66	7.71500	0.40210	2199.0	11.0	2178.0	19.0	2198	19	0.9
54	291	3.34	7.93000	0.40210	2203.0	48.0	2176.0	43.0	2240	46	2.9
91	96.3	1.37	10.41000	0.46030	2472.0	11.0	2440.0	22.0	2485	15	1.8
33	342.8	2.45	11.05000	0.45730	2528.9	8.9	2427.0	23.0	2633	15	7.8
62	278.6	1.39	14.31000	0.54170	2772.0	10.0	2790.0	26.0	2724	12	2.4
111	115.2	1.28	16.76000	0.55480	2920.0	14.0	2844.0	29.0	2960	16	3.9

APPENDIX C

U-Pb Data Table, Stanolind-Sun Perpetual Forest #1 Lower Half (4700-5230ft MD)

PFL					207/235		206/238		207/206		
Grain #	[U] ppm	U/Th	207/235	206/238	Age Ma	2σ error	Age (Ma)	2σ error	Age (Ma)	2σ error	% Disc
84	513	1.83	0.11070	0.01631	106.6	4.1	104.3	3.7	120	87	2.2
118	548	1.81	0.12920	0.01812	123.3	3.0	115.7	2.1	249	55	6.2
3	82	1.20	0.20540	0.02842	189.5	6.6	180.6	4.5	290	100	4.7
51	88.5	1.20	0.36900	0.04981	319.2	6.2	313.3	5.4	354	54	1.8
82	394	1.62	0.37510	0.05108	323.2	4.6	321.1	5.1	319	29	0.6
59	789	5.81	0.46680	0.06330	388.7	5.8	395.5	8.4	364	23	1.7
110	101.7	0.82	0.48500	0.06360	400.9	7.5	397.1	8.1	434	47	0.9
73	362	3.27	0.54100	0.06980	439.0	8.7	434.9	6.3	450	50	0.9
60	191	1.50	0.64200	0.07470	504.8	7.9	465.9	7.7	652	48	7.7
2	117.5	1.79	0.64600	0.07870	505.7	7.8	488.3	6.9	607	47	3.4
1	168	2.86	0.67500	0.08310	523.6	7.0	514.6	5.7	579	33	1.7
32	453	8.61	0.67900	0.08550	525.8	7.7	528.0	11.0	512	22	0.4
74	248	0.50	0.70200	0.08700	539.7	7.5	537.5	8.0	590	37	0.4
116	284	2.53	0.70570	0.08730	542.6	5.4	539.4	6.2	542	26	0.6
107	81.8	2.23	0.70200	0.08750	539.7	7.1	540.5	7.5	563	39	0.1
43	362	1.15	0.72000	0.08750	549.5	9.5	541.0	10.0	613	30	1.5
53	99.9	0.76	0.69500	0.08780	535.0	14.0	542.0	10.0	495	83	1.3
105	102.8	0.94	0.72700	0.08770	557.0	13.0	542.0	10.0	611	72	2.7
119	45.9	1.59	0.72400	0.08740	552.0	16.0	542.0	11.0	514	90	1.8
83	45.7	2.33	0.72700	0.08810	553.0	13.0	544.0	8.9	571	69	1.6
4	117.3	0.64	0.72200	0.08810	552.8	9.1	544.5	9.4	627	36	1.5
44	47.2	1.45	0.73700	0.08820	562.0	12.0	545.0	12.0	602	54	3.0
87	110.5	1.95	0.72300	0.08820	551.0	11.0	545.0	11.0	573	43	1.1
80	193	0.85	0.72400	0.08860	552.7	8.1	547.1	8.9	585	31	1.0
26	107.9	1.44	0.71200	0.08870	545.0	8.2	547.8	9.1	560	40	0.5
70	67.6	5.00	0.71400	0.08890	546.0	11.0	549.0	12.0	536	59	0.5
29	75.1	0.42	0.73300	0.08930	560.1	8.7	551.3	6.5	625	53	1.6
102	67.9	0.45	0.73000	0.08950	556.0	10.0	552.0	11.0	616	75	0.7
22	148.4	4.21	0.73600	0.08990	559.6	7.2	554.8	8.1	599	37	0.9
117	69.9	1.88	0.72400	0.08950	552.0	12.0	555.0	12.0	579	70	0.5
20	63.5	0.66	0.72900	0.08990	555.0	8.7	555.1	9.2	533	53	0.0
12	272	0.67	0.73920	0.09040	561.7	5.1	558.1	6.6	601	29	0.6

106	246	1.37	0.74500	0.09070	565.9	7.4	559.5	8.0	575	25	1.1
34	92	0.88	0.72700	0.09080	554.0	11.0	560.0	12.0	571	43	1.1
19	176	1.51	0.74600	0.09100	565.3	7.2	561.1	7.4	592	31	0.7
57	24.06	0.33	0.75300	0.09140	572.0	17.0	564.0	13.0	564	88	1.4
13	95	0.99	0.73100	0.09160	557.6	9.1	564.9	8.4	558	40	1.3
52	93	2.07	0.76800	0.09240	579.7	9.4	569.4	7.9	609	41	1.8
65	195	0.94	0.75400	0.09270	571.0	7.7	571.0	10.0	558	36	0.0
23	56.8	0.99	0.77300	0.09320	580.0	12.0	574.0	10.0	612	60	1.0
85	49	1.39	0.78300	0.09320	586.0	14.0	575.0	10.0	603	79	1.9
97	402.9	8.86	0.76200	0.09320	575.2	8.6	575.0	13.0	606	43	0.0
47	33.2	0.93	0.77500	0.09380	584.0	16.0	578.0	15.0	581	71	1.0
40	193	1.98	0.80200	0.09420	597.0	10.0	580.0	12.0	687	49	2.8
46	181	5.50	0.76300	0.09430	575.1	7.7	581.0	7.5	575	31	1.0
81	35.01	1.42	0.77700	0.09400	587.0	12.0	581.0	13.0	585	65	1.0
98	120.9	0.60	0.81400	0.09460	604.0	12.0	582.6	8.0	729	58	3.5
114	69.47	1.94	0.77100	0.09460	580.7	9.3	582.9	8.3	578	42	0.4
55	306	2.12	0.78000	0.09470	585.1	7.2	583.2	8.8	574	24	0.3
6	61.3	1.08	0.77000	0.09490	579.0	11.0	584.0	10.0	586	53	0.9
120	32	0.82	0.81000	0.09500	604.0	16.0	585.0	11.0	636	74	3.1
36	43.7	0.71	0.77800	0.09510	585.0	13.0	586.0	10.0	606	73	0.2
75	166	4.71	0.78400	0.09560	587.9	6.5	588.4	7.1	591	33	0.1
78	47.5	0.99	0.79400	0.09570	593.0	11.0	589.0	10.0	596	51	0.7
39	38.7	0.95	0.81500	0.09630	605.0	11.0	592.0	13.0	648	55	2.1
42	187.3	1.08	0.87900	0.09640	641.0	11.0	592.9	9.6	813	42	7.5
113	199	4.03	0.78900	0.09630	591.0	9.5	593.0	12.0	599	31	0.3
21	146	1.26	0.80000	0.09690	596.1	9.1	596.0	11.0	621	37	0.0
111	298	2.06	0.80600	0.09720	600.6	6.9	597.6	9.0	624	25	0.5
25	172	0.94	0.83700	0.09750	617.1	7.2	599.5	8.7	707	31	2.9
104	324	1.19	0.81500	0.09750	605.1	6.2	599.8	7.6	622	31	0.9
45	104	0.91	0.80700	0.09830	600.2	8.6	604.0	10.0	581	36	0.6
88	176	0.95	0.82200	0.09830	610.1	7.9	604.5	9.5	605	28	0.9
56	39.4	1.69	0.84500	0.09830	620.0	17.0	607.0	15.0	683	71	2.1
90	350	2.37	0.84200	0.10020	620.1	5.7	615.5	7.8	615	22	0.7
8	58.4	0.98	0.89900	0.10040	662.0	23.0	616.0	18.0	842	83	6.9
27	127.9	1.48	0.81700	0.10040	607.0	10.0	617.0	14.0	600	31	1.6
101	75.6	1.41	0.86200	0.10080	630.0	19.0	619.0	20.0	690	72	1.7
94	174.1	1.30	0.86200	0.10080	631.0	7.0	619.2	7.9	668	39	1.9
68	61.4	1.53	0.83400	0.10110	614.9	9.8	622.0	11.0	615	49	1.2

103	48.6	2.16	0.87700	0.10130	644.0	12.0	622.0	17.0	730	75	3.4
50	46.4	0.93	0.83200	0.10140	614.0	12.0	624.0	11.0	606	54	1.6
58	14.7	0.38	0.88700	0.10230	647.0	17.0	628.0	18.0	688	79	2.9
64	84.3	0.60	0.86900	0.10270	634.4	8.9	629.8	9.5	673	40	0.7
66	121.6	0.83	0.86200	0.10270	630.0	14.0	630.0	17.0	654	37	0.0
14	250	1.15	0.87500	0.10280	637.8	8.1	630.6	6.8	650	23	1.1
108	161	5.90	0.85600	0.10330	626.0	14.0	633.0	18.0	617	31	1.1
92	100	2.13	0.88000	0.10400	640.3	9.8	638.0	11.0	656	43	0.4
86	425	4.06	0.87400	0.10410	637.3	6.1	638.4	8.1	622	21	0.2
91	42.96	1.15	0.89300	0.10500	647.0	19.0	644.0	23.0	666	81	0.5
17	427.4	0.96	0.89600	0.10580	649.0	16.0	648.0	12.0	673	45	0.2
54	130	1.13	0.97200	0.11420	689.1	8.1	697.1	8.1	656	34	1.2
61	215	1.11	1.19200	0.13070	795.9	9.3	793.0	12.0	791	24	0.4
10	454	1.44	1.15200	0.13130	777.4	9.7	795.0	13.0	766	18	2.3
79	215	2.88	1.22100	0.13290	809.6	7.4	806.0	11.0	820	26	0.4
33	412	6.78	1.30900	0.13940	846.0	36.0	840.0	33.0	908	55	0.7
72	110.5	1.12	1.34500	0.14600	866.0	11.0	878.0	12.0	849	36	1.4
30	381.9	3.15	1.72600	0.17240	1017.8	8.1	1025.0	11.0	1022	20	0.3
76	280	1.81	2.11200	0.19800	1151.8	9.2	1164.0	14.0	1133	20	2.7
7	266	3.27	2.17000	0.20280	1171.0	8.2	1190.0	15.0	1161	17	2.5
69	120	3.15	2.83400	0.24010	1365.0	12.0	1387.0	21.0	1336	28	3.8
63	198.1	1.20	3.74300	0.26480	1583.0	16.0	1518.0	20.0	1676	29	9.4
96	123.6	0.86	4.72100	0.32020	1770.0	11.0	1790.0	22.0	1758	19	1.8
5	60	1.26	4.74000	0.31720	1771.0	18.0	1774.0	32.0	1798	21	1.3
112	174	1.08	5.23500	0.33420	1857.0	11.0	1858.0	22.0	1874	16	0.9
48	303	0.96	6.15000	0.37560	1994.0	19.0	2054.0	37.0	1933	15	6.3
89	224.9	2.55	6.78500	0.38250	2084.0	13.0	2086.0	32.0	2050	20	1.8
16	99.7	1.78	7.09000	0.39400	2123.0	23.0	2140.0	34.0	2103	19	1.8
41	119.6	1.88	6.72900	0.37210	2075.6	9.7	2039.0	20.0	2105	13	3.1
28	346	5.30	7.22200	0.40470	2138.3	9.0	2193.0	22.0	2106	12	4.1
9	100.8	1.60	6.78000	0.37970	2084.0	15.0	2074.0	31.0	2109	16	1.7
95	56.7	0.80	6.75000	0.37740	2079.0	17.0	2062.0	31.0	2109	18	2.2
67	202.5	0.95	6.90700	0.38480	2099.0	12.0	2098.0	27.0	2110	13	0.6
11	164.4	2.92	7.00200	0.38440	2112.0	13.0	2103.0	31.0	2153	15	2.3
38	305	1.95	7.79000	0.41920	2206.0	14.0	2256.0	31.0	2153	17	4.8
35	115	1.94	7.16000	0.38700	2122.0	32.0	2107.0	53.0	2154	19	2.2
109	249	2.07	7.30000	0.39580	2148.0	12.0	2148.0	29.0	2158	12	0.5
31	14.54	0.81	7.55000	0.41300	2177.0	28.0	2229.0	55.0	2161	51	3.1

62	54.5	1.22	7.64000	0.40700	2188.0	12.0	2200.0	25.0	2168	25	1.5
99	140.9	0.37	10.66000	0.46790	2493.0	21.0	2474.0	39.0	2552	25	3.1

References

Becker, T. P., Thomas, W. A., Samson, S. D., Gehrels, G. E., 2005, Detrital zircon evidence of Laurentian crustal dominance in the lower Pennsylvanian deposits of the Alleghanian clastic wedge in eastern North America: Sedimentary Geology, v. 182, no. 1-4, p. 59–86.

Becker, T. P., Thomas, W. A., Gehrels, G. E., 2006, Linking late Paleozoic sedimentary provenance in the Appalachian basin to the history of Alleghanian deformation: American Journal of Science, v. 306, p. 777-798.

Blum, M. and Pecha, M., 2014, Mid-Cretaceous to Paleocene North American drainage reorganization from detrital zircons: Geological Society of America Geology, v. 42, p. 607-610.

Christeson, G., Eddy, D., van Avendonk, H., Norton, I., Karner, G., Johnson, C., Kneller, E., Snedden, J., 2013, Deep crustal structure northeastern Gulf of Mexico: European Geosciences Union General Assembly, Abstract EGU2013–5990.

Coleman, Jr., J. L. and Coleman, C. J., 1981, Stratigraphic, sedimentologic and diagenetic framework for the Jurassic Cotton Valley Terryville massive sandstone complex, northern Louisiana: Gulf Coast Association of Geological Societies Transactions, v. 31, 71-79.

Couch, C. A., Hopkins, E. H., Hardy, P. S., 1996, Influences of environmental settings on aquatic ecosystems in the Apalachicola-Chattahoochee-Flint River basin: U.S. Geological Survey Water-Resources Investigations Report 95-4278.

Dallmeyer, R. D., 1989, Contrasting accreted terranes in the southern Appalachian Orogen, basement beneath the Atlantic and Gulf Coastal Plains, and West African orogens, Precambrian Research, v. 42, p. 387-409.

Dutton, S. P., 1987, Diagenesis and burial history of the Lower Cretaceous Travis Peak Formation, east Texas: Austin, Tex., University of Texas, Bureau of Economic Geology, Report of Investigations No. 164, 58 p.

Dutton, S. P. and Diggs, T. N., 1992, Evolution of porosity and permeability in the Lower Cretaceous Travis Peak Formation, east Texas: AAPG Bulletin, v. 76, no. 2, p. 252–269.

Dutton, S. P., Laubach, S. E., and Tye, R. S., 1991, Depositional, diagenetic, and structural controls on reservoir properties of low-permeability sandstone, Travis Peak Formation, east Texas: Gulf Coast Association of Geological Societies Transactions, v. 41, p. 209–220.

Dutton, S. P., Laubach, S. E., Tye, R. S., Baumgardner, R. W., and Herrington, K. L., 1991, Geologic characterization of low-permeability gas reservoirs, Travis Peak Formation, east Texas: Austin, Tex., University of Texas, Bureau of Economic Geology, Report of Investigations No. 204, 89 p.

Dyman, T. S., and Condon, S. M., 2006, Assessment of undiscovered conventional oil and gas resources—Lower Cretaceous Travis Peak and Hosston Formations, Jurassic Smackover Interior Salt Basins Total Petroleum System, in the East Texas Basin and Louisiana-Mississippi Salt Basins Provinces: U.S. Geological Survey Digital Data Series DDS–69–E, Chapter 5, 39 p.

Eddy, D., van Avendonk, H., Christeson, G., Norton, I., Karner, G., Johnson, C., Kneller, E., Snedden, J., 2013, Marine seismic refraction data indicate Mesozoic syn-rift volcanism and seafloor-spreading in the northwestern Gulf of Mexico: European Geosciences Union General Assembly, Abstract EGU2013–3607.

Ewing, T. E., Lopez, R. F., 1991, Principal structural features, the Gulf of Mexico basin, Plate 2: The Geology of North America, v. J, Geological Society of America.

Ewing, T. E., 2010, Pre-Pearsall Geology and Exploration Plays in South Texas: Gulf Coast Association of Geological Societies Transactions, v. 60, p. 241-260.

Farre, J.A., McGregor, B.A., Ryan, W.B.F., Robb, J.M., 1983, Breaching the shelfbreak passage from youthful to mature phase in submarine canyon evolution: SEPM Special Publication 33, 25–39.

Fiduk, J. C., Anderson, L. E., Rowan, M. G., 2004, The Wilcox raft: an example of extensional raft tectonics in south Texas, northwestern onshore Gulf of Mexico: Proceedings of the Twenty-fourth Annual Gulf Coast Section SEPM Foundation Bob F. Perkins Research Conference, Dec. 5-8, 2004.

Fiduk, J. C., Clippard, M., Power, S., Robertson, V., Rodriguez, L., Ajose, O., Fernandez, D., Smith, D., 2014, Origin, transportation, and deformation of Mesozoic carbonate rafts in the northern Gulf of Mexico: Gulf Coast Association of Geological Societies Journal, v. 3, p. 20-32.

Galloway, W. E., 2002, Cenozoic deep-water reservoir systems of the northern Gulf of Mexico Basin: Gulf Coast Association of Geological Societies Transactions, v. 52, p. 301-308.

Galloway, W. E., 2008, Depositional Evolution of the Gulf of Mexico Sedimentary Basin: Sedimentary Basins of the World, Chapter 15, v. 5, 45 p.

Ge, H., Jackson, M. P. A., Vendeville, B. C., 1997, Kinematics and Dynamics of Salt Tectonics Driven by Progradation: AAPG Bulletin, v. 81, no. 3, p. 398-423.

Gorsline and Emery, 1959 Gorsline, D. S., and K. O. Emery, 1959, Turbidity-current deposits in San Pedro and Santa Monica basins off southern California: Geological Society of America Bulletin, v. 70, p. 279–290.

Heatherington, A. L. and Mueller, P. A., 2003, Mesozoic Igneous Activity in the Suwannee Terrane, Southeastern USA: Petrogenesis and Gondwanan Affinities: Gondwana Research, v. 6, no. 2, p. 296–311.

Herron, D. A., 2014, Thoughts and Observation on Interpreting Depth-Imaged Data in the Jurassic Norphlet Play, Deepwater Eastern Gulf of Mexico: AAPG Search and Discovery Article 41342, 16 p.

Hudec, M. R., Norton, I. O., Jackson, M. P. A., Peel, F. J., 2013, Jurassic evolution of the Gulf of Mexico salt basin: AAPG Bulletin, v. 97, no. 10, p. 1683-1710.

Kumar, N., and R. M. Slatt, 1984, Submarine-fan and slope facies of Tonkawa (Missourian-Virgilian) sandstone in deep Anadarko basin: AAPG Bulletin, v. 68, p. 1839–1856.

Lisi, A. F., 2012, Provenance of the Upper Jurassic Norphlet and surrounding formations from U-Pb detrital zircon geochronology: West Virginia University, 148 p.

Lomando, A.J., 1992, The influence of solid reservoir bitumen on reservoir quality: AAPG Bulletin, v. 76, no. 8, p. 1137–1152.

Mancini, E. A., Mink, R. M., Bearden, B. L., Wilkerson, R. P., 1985, Norphlet Formation (Upper Jurassic) of southwestern and offshore Alabama: Environments of deposition and petroleum geology: AAPG Bulletin, v. 69, no. 6, p. 881-898.

Mancini, E. A., Mink, R. M., Bearden, B. L., Mann, S. D., Bolin, D. E., 1990, Desert environments and petroleum geology of the Norphlet Formation, Hatter's Pond field, Alabama, in J. H. Barwis, J. G. McPherson, and J. R. J. Studlick, eds., Sandstone petroleum reservoirs: New York, Springer-Verlag, p. 153–180.

Marzano, M. S., Pense, G. M., Andronaco, P., 1988, A comparison of the Jurassic Norphlet formation in Mary Ann Field, Mobile Bay, Alabama to onshore regional Norphlet trends: Gulf Coast Association of Geological Societies Transactions, v. 38, p. 85-100.

McDonnell, A., 2010, Salt-sediment interactions during the Jurassic to the Miocene of Mississippi Canyon area, northern Gulf of Mexico: Applied Geodynamics Laboratory 23rd Annual Review Meeting, 34 slides.

Mitchum, Jr., R. M., Sangree, J. B., Vail, P. R., Wornardt, W. W., 1994, Recognizing sequences and systems tracts from well logs, seismic data, and biostratigraphy: Examples from the Late Cenozoic of the Gulf of Mexico, in Weimer, P. and Posamentier, H. W., eds, AAPG Memoir 58, p. 163-197.

Moore, C. H., 1984, The Upper Smackover of the Gulf Rim: Depositional systems, diagenesis, porosity evolution and hydrocarbon production: GCSSEPM Foundation Third Annual Research Conference Proceedings, p. 283-307.

Moore, G. T., 1969, Interaction of rivers and oceans; Pleistocene petroleum potential: AAPG Bulletin, v. 53, p. 2421-2430.

Mullins, H. T. and Cook, H. E., 1986, Carbonate apron models: Alternatives to the submarine fan model for paleoenvironmental analysis and hydrocarbon exploration: Sedimentary Geology, v. 48, p. 37-79.

Olson et al., in press, Interpretation: vol. 3, no. 2 (May 2015); p. 1–20, 15 figs., 1 table.

Park, H., Barbeau Jr., D. L., Rickenbaker, A., Bachmann-Krug, D., Gehrels, G., 2010, Application of Foreland Basin Detrital-Zircon Geochronology to the Reconstruction of the Southern and Central Appalachian Orogen: The Journal of Geology, v. 118, no. 1, p. 23–44.

Patruno, S., Hampson, G. J., Jackson, C. A. L., Quantitative characterization of deltaic and subaqueous clinoforms: Earth-Science Reviews, v. 142, p. 79-119.

Pilcher, R. S., Murphy, R. T., Ciosek, J. M., 2014, Jurassic raft tectonics in the northeastern Gulf of Mexico: Interpretation, v. 2, no. 4, p. SM39-SM55.

Playton, T. E., Janson, X., Kerans, C., 2010, Carbonate Slopes, in James, N. P., and Dalrymple, R. W., eds., Facies Models 4: Geological Society of Canada, p. 449-476.

Puga-Bernabéu, A., Webster, J. M., Beaman, R. J., Guilbaud, V., 2011, Morphology and controls on the evolution of a mixed carbonate–siliciclastic submarine canyon system, Great Barrier Reef margin, north-eastern Australia: Marine Geology, v. 289, p. 100-116.

Reading and Richards, 1994, Turbidite systems in deep-water basin margins classified by grain size and feeder system: AAPG Bulletin, v. 78, p. 792-822.

Russell, R. D., 1939, Effects of transportation of sedimentary particles, in Trask, P. D., ed, Recent Marine Sediments, The Society of Economic Paleontologists and Mineralogists, p. 32-47.

Salvador, A., 1987, Late Triassic-Jurassic Paleogeography and Origin of Gulf of Mexico Basin: AAPG Bulletin, v. 71, no. 4, p. 419–451.

Saucier, A.E., 1985, Geologic framework of the Travis Peak (Hosston) Formation of east Texas and northern Louisiana, in Finley, R.J., Dutton, S.P., Lin, Z.S., and Saucier, A.E., eds., The Travis Peak (Hosston) Formation—Geologic framework, core studies, and engineering field analysis: Austin, Tex., University of Texas, Bureau of Economic Geology, contract report prepared for the Gas Research Institute under contract no. 5082-211-0708, 233 p.

Saucier, A.E., Finley, R.J., and Dutton, S.P., 1985, The Travis Peak (Hosston) Formation of east Texas and northern Louisiana, in Proceedings, 1985 Society of Petroleum Engineers/ Department of Energy Joint Symposium on Low-Permeability Reservoirs: Society of Petroleum Engineers/U.S. Department of Energy Paper No. 13850, p. 15–22.

Scott, T. M., 1988, The lithostratigraphy of the Hawthorn Group (Miocene) of Florida: Florida Geological Survey Bulletin No. 59, 167 p.

Snedden, J. W., Norton, I. O., Christeson, G. L., Sanford, J. C., Interaction of deepwater deposition and a mid-ocean spreading center, eastern Gulf of Mexico basin, USA: Gulf Coast Association of Geological Societies Transactions, v. 64, p. 371-383.

Snedden, J., Eddy, D., Christeson, G., van Avendonk, H., Olson, H., Ganey-Curry, P., Norton, I., 2013, A new temporal model for eastern Gulf of Mexico Mesozoic deposition: Gulf Coast Association of Geological Societies Transactions, v. 63, p. 609–612.

Snedden, J. W., Galloway, W. E., Whiteaker, T. L., Ganey-Curry, P. E., 2012, Eastward shift of deepwater fan axes during the Miocene in the Gulf of Mexico: Possible causes and models: Gulf Coast Association of Geological Societies Journal, v. 1., p. 131-144.

Snedden, J., Liu, C., 2010, A compilation of Phanerozoic sea level change, coastal onlaps, and recommended sequence designations: AAPG Search and Discovery Article 40594, 3 p.

Snedden, J. and Olson, H., pers. comm.

Snedden, J., Gulf Basin Depositional Synthesis Phase IX, Hosston Paleogeography, unpublished map.

Somme, T. O., Helland-Hansen, W., Martinsen, O. J., Thurmond, J. B., 2009, Relationships between morphological and sedimentological parameters in source-to-sink systems: a basis for predicting semi-quantitative characteristics in subsurface systems: Basin Research, v. 21, p. 361-387.

Stow, D. A. V., 1981, Laurentian Fan: morphology, sediments, processes and growth pattern: AAPG Bulletin, v. 65, p. 375–393.

Tsikalas, F., Faleide, J. I., Eldholm, O., Blaich, O. A., 2012, The NE Atlantic conjugate margins, in Roberts, D. G., Bally, A. W., eds, Regional geology and tectonics: Phanerozoic passive margins, cratonic basins and global tectonic maps, Chapter 5, 48 p.

Turner, P., 1948, Alluvial Red Beds: Continental Red Beds, Chapter 4, v. 29, 86 p.

Tye, R.S., 1991, Fluvial sandstone reservoirs of the Travis Peak Formation, East Texas Salt Basin, in Miall, A.D., and Tyler, N., eds., The three-dimensional facies architecture of terrigenous clastic sediments, and its application for hydrocarbon discovery and recovery: SEPM (Society of Sedimentary Geology) Concepts in Sedimentology and Paleontology, v. 3, p. 172–188.

van Avendonk, H., G. Christeson, I. Norton, D. Eddy, G. Karner, C. Johnson, and E. Kneller, 2013, Structure and evolution of the Gulf of Mexico: New results from the GUMBO marine seismic refraction study: European Geosciences Union General Assembly, Abstract EGU2013–6230.

Wezel, F. C., Savelli, D., Bellagamba, M., Tramontana, M., Bartole, R., 1981, Plio-Quaternary depositional style of sedimentary basins along insular Tyrrhenian margins, *in* Wezel, F. C., ed., Sedimentary basins of Mediterranean margins: CNR Italian Project of Oceanography, p. 239–269.

Wilson, J. L., Ward, W. C., Finneran, J., 1984, A field guide to Upper Jurassic and Lower Cretaceous carbonate platform and basin systems Monterrey-Saltillo area, northeast Mexico: Gulf Coast Section, Society of Economic Paleontologists and Mineralogists Foundation, San Antonio, Texas, 81 p.

Winston, G. O., 1976, Florida's Ocala Uplift is not an uplift: AAPG Bulletin, v. 60, no. 6, p. 992-994.

Vita

Ann Caroline Bovay was born and raised in Gainesville, Florida. She graduated from Washington and Lee University in Lexington, Virginia with a Bachelor of Science in Geology, with honors, *cum laude*. During her senior year at Washington and Lee, she realized that she wanted to give back to the place that gave her so much, and worked in University Advancement as an Assistant Director of Annual Giving. It only took one meeting with one alumnus, the Chairman of Indigo Minerals, LLC, for her to realize that the next time she was in a geologist's office she wanted to be talking about rocks, not gifts. Caroline decided to return to geology and attend The University of Texas at Austin, always her top choice for graduate studies in geological sciences, to complete a Master of Science in Geological Sciences focusing on clastic sedimentology and stratigraphy in deep-water systems.

Permanent email address: cbovay@utexas.edu

This thesis was typed by Ann Caroline Bovay.